

2009

The 5' Bop Gene Stem-Loop Sequence: Stability, Structure, and Function

Srikanth Tangeloju
Seton Hall University

Follow this and additional works at: <https://scholarship.shu.edu/dissertations>

Part of the [Biology Commons](#), and the [Genetics and Genomics Commons](#)

Recommended Citation

Tangeloju, Srikanth, "The 5' Bop Gene Stem-Loop Sequence: Stability, Structure, and Function" (2009). *Seton Hall University Dissertations and Theses (ETDs)*. 2464.
<https://scholarship.shu.edu/dissertations/2464>

**The 5' bop gene Stem-Loop Sequence:
Stability, Structure, and Function**

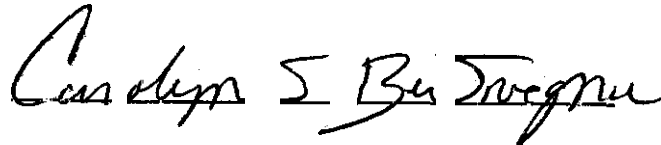
by

Srikanth Tangeloju

M.S. Thesis

**Submitted to the Department of Biology of Seton Hall University
in partial fulfillment of the requirement for the degree of Master of Science.**

Approved by:

A handwritten signature in black ink that reads "Carolyn S Bentivegna". The signature is written in a cursive style with a large initial 'C' and 'B'.

Carolyn S Bentivegna, Ph.D.

Mentor

Yufeng Wei, Ph.D.

Committee Member

Jane L Ko, Ph.D.

Committee Member

TABLE OF CONTENTS

Dedication	4
Acknowledgement.....	5
List of tables.....	6
List of Figures	7
Abstract.....	8
Introduction.....	10
Materials and Methods	27
Results	37
Discussion	48
Summary	51
Literature Cited	55
Annexure I	59
Annexure II	64

DEDICATION

My family and friends

ACKNOWLEDGEMENT

I would like to sincerely thank the faculty at Seton Hall University, especially Dr Turner for his support as a Mentor. I would like to take this opportunity to extend my heart felt thanks to Dr Bentivegna for her support as my thesis mentor and her invaluable guidance, when everything else seemed impossible to me. I would also like to thank Dr Jane Ko and Dr Yufeng Wei for their guidance and encouragement during the completion of the project.

I would also like to acknowledge my family and friends (especially Vijay Bhaskar Reddy) for the enormous amount of faith in me. Lastly I would like to thank Shirisha Chittiboyina for being the main reason behind my pursuit of science.

LIST OF TABLES

1. Mutant sequences
2. ΔG & T_m values calculated using Mfold.
3. The Mfold thermodynamics predictions (Annexure II)
 - a. WT
 - i. Structure 1
 - ii. Structure 2
 - b. C2A Structure
 - c. G8A
 - i. Structure 1
 - ii. Structure 2
 - iii. Structure 3
 - iv. Structure 4
 - d. A10C
 - i. Structure 1
 - ii. Structure 2
 - e. G11A
 - i. Structure 1
 - ii. Structure 2
 - f. G11C
 - i. Structure 1
 - ii. Structure 2
 - g. A14G
 - i. Structure 1
 - ii. Structure 2
 - h. DM
 - i. Structure 1
 - ii. Structure 2
 - iii. Structure 3
 - iv. Structure 4
 - v. Structure 5
 - i. TM
 - i. Structure 1
 - ii. Structure 2
 - iii. Structure 3
 - iv. Structure 4

LIST OF FIGURES

1. The seven transmembrane structure of bR
2. The bacterio-opsin gene
3. Stem loop mutants
 - a. Wild type, G11A, G11C, C2A and T6C
 - b. WT, A10C, A14G, G8A, T6C:G8C and T6C:G8C:A20C
4. Cloning and expression vector
 - a. The cloning vector (pENDS) and the expression vector (pHex)
 - b. The pHex and pENDs analytical digest.
5. The *PstI* -*BamHI* fragment of the pENDS vector XXI showing the restriction sites
6. The *PstI* - *BamHI* fragment of the pENDS vector VII showing the restriction sites
7. Average ΔG values of different mutants calculated using Mfold.
8. Restriction digests of pENDs vector (pENDs XXXI)
9. Restriction digests of pENDs vector (pENDs VII)
10. Representative gel showing the *PstI* and *BamHI* fragment.
11. *PstI* - *BamHI* fragment before transformation into *Halobacterium salinarum*
12. *Pst I* - *BAM HI* digest of the DNA from *Escherichia coli*(*E.coli*)
13. Colony image of the mutants transformed into L33
14. Integrated density of the colony images.
15. Growth curves of the mutants.
16. Br quantification of mutants C2A, G1 1A and G1 1C in comparison with the wild type

Abstract

In pursuit of GPCR characterization, our lab chose to work with a model organism *Halobacterium salinarum* (*H. sal.*). This organism contains the bacterioopsin gene (*bop*), which encodes the protein precursor of the purple membrane protein bacterioopsin (Bop). The bacterioopsin gene (*bop*) was chosen as the reporter for the study. The putative stem-loop structure within the *bop* gene is considered to be a key component of the molecular machinery that regulates Bop synthesis. Previous work in our lab has indicated that single base pair disruptions dramatically reduced stem-loop stability (differential scanning calorimetry (DSC), circular dichroism (CD) and ultraviolet (UV) spectroscopy analysis). The work presented here evaluated the influence of cooperative base pairing on stem-loop stabilization (Mfold algorithm predictions) and the relationship between stem-loop stability and bR production *in-vivo*. The approach involved subcloning mutant oligomers into a vector designated as pENDS and subsequently cloning the product into an expression vector designated as pHex. The pHex vector was then expressed in *H. sal.* In order to check the validity of the cloning, the vector was transformed back into *E. coli* and the plasmid DNA was extracted and sequenced. Results of this preliminary mutational study of the 5' *bop* gene stem-loop structure indicated that the stem-loop is indeed present *in-vivo* in *H. sal.* Further the study indicated that an increase in the stability of the stem-loop decreases the production of bR significantly, and the decrease in the stability of the stem-loop also decreases the production of bR. The decrease in stability was not directly proportional to the increase in predicted ΔG value. However, the increase in stability was directly proportional to the decrease in the predicted ΔG value. This work has found a correlation between the stem-

loop structural stability and bR accumulation, thereby demonstrating that molecular machinery responsible for the production of bR in *Hsal* is highly optimized. More quantitative methods like mRNA analysis can be used to further establish these findings.

Introduction

G-Protein Coupled Receptors (GPCR) comprise the single largest category of sensory receptors. The role of GPCR in relation to normal cellular function has been well established(1). At least 1000 subtypes of these receptors have been identified and the function of at least 200 of these receptors is already known. Defective signaling related to a GPCR can lead to diseases like congestive heart failure, schizophrenia, high blood-pressure, allergic reactions, stroke, cognitive disorders, and blindness (2, 3). Nearly 60 percent of all prescribed drugs target GPCR either directly or indirectly and account for nearly 200 billion US dollars in sales per year (4). However our understanding of GPCR receptors is limited because of the lack of knowledge about the structure and structural changes that are related to receptor activation.

GPCRs are extremely sensitive and hence are produced by individual cells at extremely low levels so as to not overwhelm all the other cellular functions(5). However this low abundance of receptor species in cells is a major obstacle for scientific analysis of their mechanisms of action. Numerous laboratories have been trying to obtain receptor (GPCR etc) in quantities required for their purification and physical analysis (6, 7). The visual pigment bovine rhodopsin (8-11) and the β 2 adrenergic receptor (12) are amongst the few GPCR whose structures are known at the atomic level. Characterization of most GPCR structures have therefore relied on sequence homology alignments (13, 14), predictive secondary structural algorithms (15) and mutagenesis (16-19). Hence a logical approach would be to exploit a system that produces the receptor in the required quantities and to use methods such as genetic engineering on these systems in order to understand the structure and functionality of the receptor. In pursuit of this strategy my

work in our laboratory would like to exploit the molecular machinery of a relatively new expression system *H.salinarum* (*Hsal*), which is responsible for naturally producing membrane protein bacteriorhodopsin (bR).

Bacteriorhodopsin (bR)

bR shares structural similarities with GPCR because of its seven transmembrane motif (Figure 1). Proteomic and genomic analyses of the GPCR indicate a presence of an intracellular carboxyl-terminus (C-terminus) (14), an extracellular amino-terminus (N-terminus) and a seven alpha-helical transmembrane spanning domains (7TM). The secondary structure of bR is predicted to be similar to that of GPCR.(13)

Figure 1: The seven transmembrane structure of bR (20). The transmembrane helices are shown in red. The outside of the cell is at the bottom and inside of the cell is at the top.

bR is the sole membrane protein produced by the bacterio-opsin gene (*bop*) (21). Bacteriorhodopsin is a 26 kilo dalton (kDa) transmembrane protein that acts as a light-driven proton pump, converting light energy into a proton gradient. bR is the simplest known light driven proton pump (22). Under low nutrient, high light, and decreased

oxygen conditions, the host organism, *Halobacterium salinarum*, uses this proton pump to support its energy requirement. bR is induced by more than 50 fold under low-oxygen conditions (23, 24). bR is a single polypeptide (bacterio-opsin, Bop) of 248 amino acids. These amino acids are arranged in seven alpha-helical transmembrane spanning domains. These helices in-turn enclose a retinal chromophore linked via a protonated Schiff base to residue Lys216 of the seventh transmembrane helix of the bacterio-opsin (25). The retinal, upon absorption of a photon, undergoes isomerization from the all-trans to the 13 cis configuration (26) (Figure 1). The retinal chromophore and the 248 amino acids are in a 1:1 assembly (27). The chromophoric properties of the retinal cause the *H. salinarum* culture to be intensely purple in color and thereby provide a visual assay of expression (28). bR is expressed at 15-30 mg per liter of culture, which is considered as an extraordinary level of membrane protein production (29). These levels of bR accumulation makes one believe that the molecular machinery of bR production has been highly optimized. *In lieu* of the above factors, I hypothesize that the bacterio-opsin gene structure has been highly optimized to achieve maximal levels of bR accumulation.

Halobacterium salinarum

The archaeon *Halobacterium salinarum* is an extremely halophilic and rod shaped archaea found in evaporating salt ponds. Archaea is a phylogenetically distinct group of prokaryotic organisms. Archaea is as distantly related to humans as they are with other bacteria (30). In Archaea, the Shine Dalgarno sequence is upstream of the initiation codon, and it has a leaderless mRNA. *H.salinarum* expresses extremely high amounts of bR under intense light and/or anaerobic conditions. bR occupies 80 percent of the cell membrane in *H.sal* and can be purified to yield up to 15-30 milligrams per liter of cell

culture (28, 31). Further, bR accumulation is low under aerobic conditions. However *H.salinarum*'s viability is independent of bR accumulation, and hence the cell membrane may be made available to express non native receptor proteins (32). As mentioned above, bR is a structural homologue of GPCR. Hence it was logical for me to exploit *H.salinarum* in order to study the over expression of bR. There are some notable differences between bR and GPCR. For example, bR has smaller N and Carboxy terminii compared to GPCR (33). However understanding the molecular mechanism for the expression of the bacterio-opsin (*bop*) gene should be useful for determining what factors influence the high production of bR in *H.sal*. This knowledge can be later extrapolated to the GPCR machinery and/or might be useful for *in vitro* production of other homologous mammalian GPCR membrane proteins.

H.sal is considered ideal for this study. First, *H.sal* can be manipulated similarly to *E.coli* (28, 31). Second, all the vectors for gene transfer of bR and GPCR have been previously developed in *H.sal* (34). Third, *H.sal* does not have G-protein signal transduction components and hence an over expression or no expression of transgenic GPCR might not affect the cellular physiology and viability of the organism. Further, being a member of archaea, *H.sal* has both prokaryotic and eukaryotic traits and hence an understanding of this organism might facilitate the expression of protein from both the prokaryotic and eukaryotic domains (35, 36).

The *bop* gene

The bacterio-opsin gene (*bop* gene) consists of 832 base pairs (bp). The *bop* gene has been sequenced. Its transcriptional promoter, putative regulatory factor binding sites and transcription termination sites have been previously identified (29, 37, 38). It is also

well understood that there is dedicated molecular machinery for insertion of the bR into the cell membrane. The first 11 *bop* amino acids function as a signal sequence thereby coupling bR to the cell membrane (39).

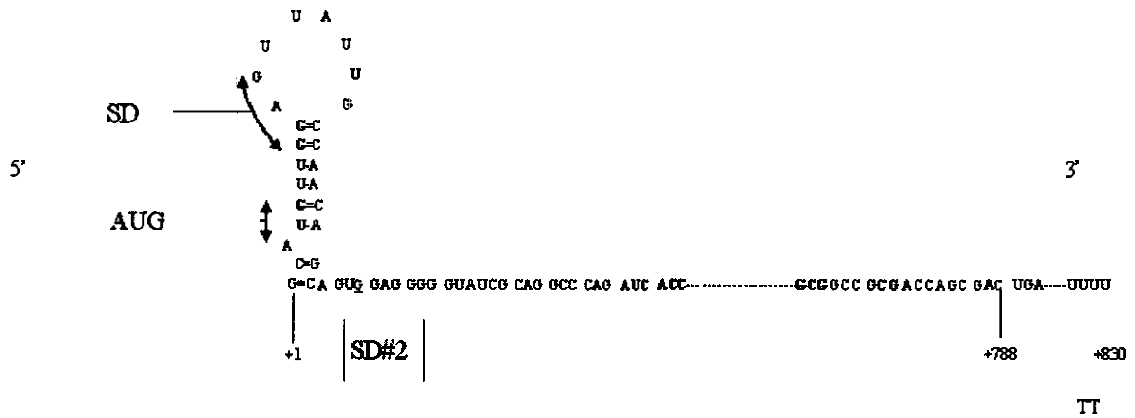


Figure 2a: The bacterio-opsin gene, the 832 bp mRNA. The stem loop region is shown with the corresponding nucleotides within the stem loop. The AUG and the SD#1 and the SD#2 are shown in the figure.

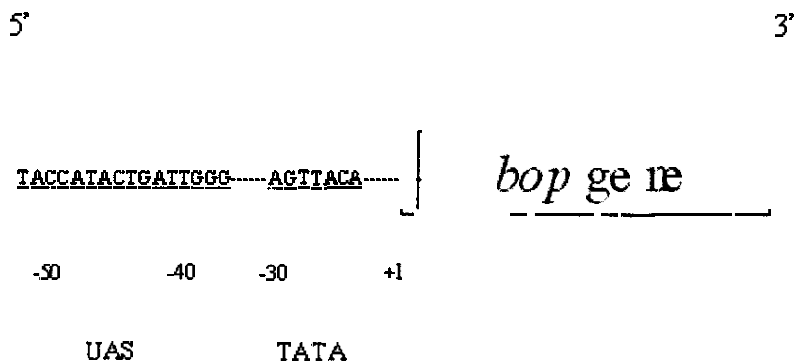


Figure 2b: The *bop* gene. Upstream activator site (UAS) and a TATA box are present towards the 5' end of the *bop* gene. (38)

The 5' end of the *bop* gene was the major focus for my study. This 5' end has a putative stem and a loop structure (called the stem-loop). The stem-loop is formed by twenty five bases of the *bop* mRNA and consists of an intramolecular anti parallel duplex (stem) and has a certain number of unpaired nucleotides (loop). The GC triple bonds, the AT double bonding, along with the hydrogen bonds (in mutants like A10C) should stabilize this stem-loop region of the *bop* gene. The stem loop has 2 Shine Dalgarno (SD) sites and a start codon (AUG). The UAS is observed around 35 bp upstream of the AUG, and the TAT is observed at 830 bp downstream of AUG.

Further, using twenty five synthetic oligonucleotides (GCATGTTGGAGTTATTGCCAACAGC), representing the wild type stem-loop structure, our lab (Maged Darwish, Mike Arent, Coz Antonaci unpublished) previously established the presence of a putative stem loop structure. Ultraviolet spectroscopic studies involving the T_m of these twenty five nucleotides showed the presence of a hyperchromic transition. Hyperchromic transition is the increase in UV light caused by the breakage in bonds between the nucleotides of the stem region of the stem-loop. The Circular Dichroism Spectroscopy studies on the twenty five nucleotides indicated that this hyperchromic transition involves a loss of helical character. The Differential Scanning Calorimetry indicated that there is indeed a thermodynamic fingerprint defined in terms of ΔG , ΔS , and ΔH . Hence the next logical question was to understand the interaction between the nucleotides of the 5' *bop* gene stem loop sequence and their role in determining stability, structure, and function.

The stability of this stem loop is considered to be a major factor for bR production. Further the role of the two SD in bR accumulation was previously unclear.

Hence one of the major objectives of my study was to understand how the nucleic acid sequences in the stem loop region of the 5' end of the *bop* gene coding region affects bR accumulation.

The factors which affect the bR accumulation in *H.sal* can be broadly categorized into 2 types as follows (40):

a. Trans-acting “determinants”: The trans-acting determinants can be considered as external factors (like light and oxygen). For example intense light and/or a decrease in oxygen have a direct effect on the amount of *bop* messenger RNA (mRNA) (27). Trans-acting determinants also include factors which are not part of the *bop* gene nucleic acid sequence. There are two purine rich regions at the 5' end of the gene which are referred (Figure 2) to as Shine-Dalgarno (SD) sites. Complementary to this SD region is the anti-shine dalgarno site (aSD), a highly conserved pyrimidine rich region at the 3' end of all 16S ribosomal RNAs (41, 42). The SD sites in eubacterial organisms recruit ribosomes (via their component 16S ribosomal RNA) to mRNA to initiate translation of mRNA (43). Hence the aSD sequence on the 16S rRNA may also be a trans-acting determinant of *bop* gene expression i.e aSD on the 16s rRNA is an external factor for bR accumulation.

b. Cis-acting “determinants”: Cis-acting determinants are factors that are an integral part of the *bop* gene nucleic acid sequence. The mRNA of the *bop* gene starts just two nucleotides upstream of the first translation initiation codon (methionine) (44), because of this, all the cis-acting determinants in the *bop* mRNA are located downstream of the initiation codon. The *bop* gene has two putative SD sites. The first SD (SD#1) site is located in the loop region of the putative secondary structural element (stem-loop) and

the second SD (SD#2) is located immediately downstream of the stem-loop (Figure 2). The two putative SD sites follow the AUG (start codon), which is quite intriguing for a prokaryotic translational mechanism, since the canonical translational initiation mechanisms invoke ribosome binding upstream of the AUG. This type of molecular mechanism where the ribosome binds upstream to the AUG site is a rare architecture in eukaryotes and prokaryotes (including archaea) (45). The 5' stem-loop structure and the *bop* gene SD sites are cis-acting determinants of expression, and I hypothesize that their rare architecture accounts for the unusually high levels of *bop* protein.

My objectives specifically focused on the Cis acting determinants of the *bop* gene. The roles of both the cis-acting and trans-acting determinants are still hypothetical because the determinants discussed above have not been confirmed experimentally.

My specific aims were

1. To determine if the putative stem loop structure exists *in-vivo*.
2. To understand the 5' end of the bop gene stem-loop sequence in terms of its stability, structure, and function.
 - a. the role of the nucleotide interactions in the stem loop (cis-acting determinants)
 - b. M-fold analysis to supplement the *in-vitro* studies

Mutants:

The stem loop consists of twenty five nucleotides. The stem loop starts at two nucleotides upstream of ATG. The twenty five nucleotides of the stem loop sequence are GCATGTTGGAGTTATTGCCAACAGC. Different mutational sites were chosen in order to evaluate nucleotide interactions in the stem-loop and SD regions. The mutants were designed at the DNA level so that the corresponding transcribed mRNA could be studied *in-vivo*. Mutants are depicted in Figures 3a and 3b and the predicted secondary structure of these mutants are depicted in Annexure II.

(a) Wild type oligomer is used to establish baseline values to which the other mutant oligomers are compared. (b) C2A is a mutant oligomer where the Cytosine (C) at the second location is mutated to an Adenosine (A). The Mfold algorithm (explained below) predicts the structure of this mutant to be similar to one of the probable two structures of the wild type. (c) T6C is a mutant oligomer where the Thymine (T) at the sixth location is mutated to Cytosine (C). This mutant is expected to destabilize the stem loop region. (d) G8A is a mutant oligomer where the Guanine (G) at the eighth location is mutated to Adenosine (A). This mutation is expected to create a mismatch in the stem portion of the 5' end of the *bop* gene and thereby decrease the stability of the stem-loop. (e) A10C is a mutant oligomer where the Adenosine (A) is replaced with Cytosine(C) at the tenth location in the stem loop. This mutant is expected to increase the stability of the stem loop. Mfold analysis predicts that the ΔG value of A10C is significantly lower than the other mutants. A10C creates an additional C-G base pairing in the loop region and thereby is expected to stabilize the stem-loop structure of the *bop* gene. The mutant oligomer A10C also perturbs the SD site. (f) G11A is a mutant where the Guanine (G) is

mutated to Adenosine (A) at the eleventh location. This structure perturbs the SD site and also causes the destabilization of the stem-loop structure. (g) G11C is a mutant where the Guanine (G) is mutated to Cytosine (C) at the eleventh location. This mutant perturbs the SD structure and also causes the destabilization of the stem loop structure. This mutant can be compared with G11A to better understand the importance of specific nucleotide interactions. This mutant also changes the translated amino acid from Glutamate to Alanine. Though both Glutamate and alanine are acidic amino acids, the difference in the number of carbons might have an effect on the bR (h) A14G is a mutant with Adenosine (A) at the fourteenth location mutated to Guanine (G). This mutant acts as a control because it does not effect the SD site and it does not effect the base pairing in the stem-loop region (i) T6C: G8C is called a double mutant (DM) because it has mutations in two locations: the first mutation is in the sixth location where an Thymine (T) is mutated to Cytosine (C) and the second mutation is at the eighth location where Guanine (G) is mutated to Cytosine (C). This mutation is expected to destabilize the stem-loop structure, because of the decrease in the base pairing. Mfold analysis predicts the increase in the ΔG for this mutant. This mutant will help understand the effect of a double destabilization versus a single destabilization. (j) T6C:G8C:A20C is termed as a triple mutant (TM) because it has mutations in three locations: the Thymine (T) at sixth location is mutated to Cytosine (C), the Guanine (G) at the eighth location is mutated to Cytosine (C) and the Adenosine (A) at the twentieth location is mutated to Cytosine (C). This mutation will help understand the effect of a triple destabilization versus a single or a double destabilization.

The sequences for all mutants are given below.

WT VII
TTACACACAGATCTTCGTTAGGTA**CT**GTTGCATGTTGGAGTTATTGCC
AACAGCAGTGGATATCGTATCGC

WT XXXI
TTACACACAGATCTTCGTTAGGTA**CT**GTTGCATGTTGGAGTTATTGCC
AACAGCAGTGGATATCGTATCGC

M2 C2A
TTACACACAGATCTTCGTTAGGTA**Ga**ATGTTGGAGTTATTGCCA
ACAGCAGTGGATATCGTATCGC

M6 T6C
TTACACACAGATCTTCGTTAGGTA**Gc**TGGAGTTATTGCC
AACAGCAGTGGATATCGTATCGC

M8 G8A
TTACACACAGATCTTCGTTAGGTA**Ta**GAGTTATTGCCA
ACAGCAGTGGATATCGTATCGC

M10 A10C
TTACACACAGATCTTCGTTAGGTA**Gc**GTTATTGCCA
ACAGCAGTGGATATCGTATCGC

M11 G11A
TTACACACAGATCTTCGTTAGGTA**Aa**TTATTGCCA
ACAGCAGTGGATATCGTATCGC

M11 G11C
TTACACACAGATCTTCGTTAGGTA**Gc**TTATTGCCA
ACAGCAGTGGATATCGTATCGC

M14 A14G
TTACACACAGATCTTCGTTAGGTA**Gg**TGGAGTTATTGCCA
ACAGCAGTGGATATCGTATCGC

DM T6C:G8C
TTACACACAGATCTTCGTTAGGTA**GcTa**GAGTTATTGCCA
ACAGCAGTGGATATCGTATCGC

TM T6C:G8C:A20C
TTACACACAGATCTTCGTTAGGTA**GcTa**GAGTTATTGCC**c**
ACAGCAGTGGATATCGTATCGC

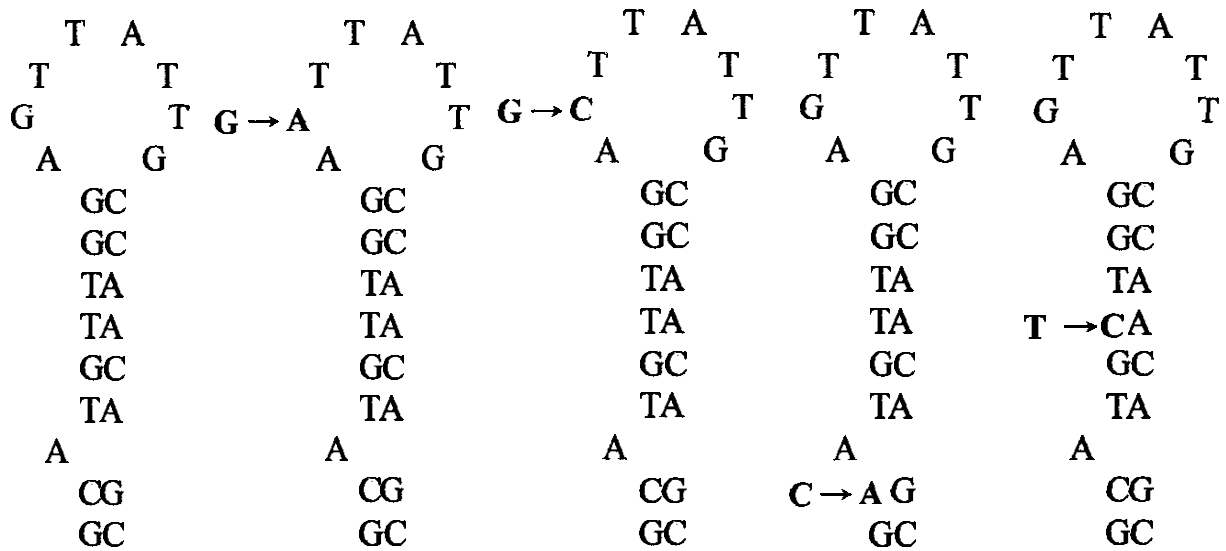


Figure 3a: Stem loop mutants – Wild type (WT), G11A, G11C, C2A and T6C.

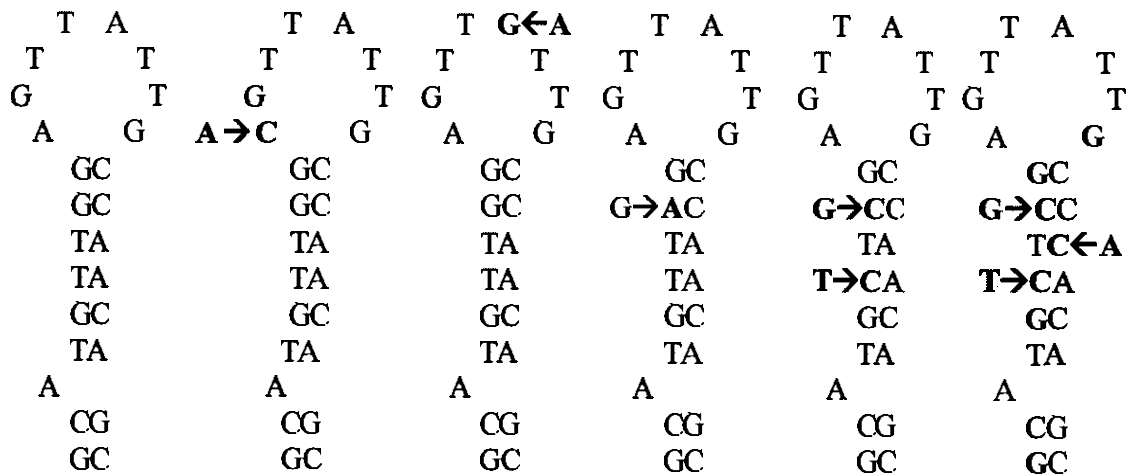


Figure 3b: Stem loop mutants – WT, A10C, A14G, G8A, T6C:G8C and T6C:G8C:A20C

The predicted structures for the mutants (Mfold analysis) are shown in Annexure II.

The design of the stem loop mutant oligomers were such that they would not affect the amino acid sequence of the N terminal portion of the resultant bR protein, i.e. all the mutants except A10C and G11C were designed so that only the wobble base of each codon was changed. This means that the mutated oligomer would code for the same amino acid as in the wild type. Since the amino acid of the coded bR is the same as that of the wild type, any perturbations (or its absence) can be attributed to the stability of the stem loop region. The exception is the A10C and G11C, this mutation would affect the amino acid produced. Further, the mutant oligomers and their complementary strands have the appropriate flanking sequences which allow them to be cloned into the *bop* gene vector. However there might be some loss of membrane insertion of bR caused by mutation of the 5' end of the mRNA i.e the bR might be produced but might not get inserted into the membrane due to the perturbations in the signaling sequences.

Vectors:

A. Subcloning into the cloning vector (pENDs)

The mutants (as explained above) were generated using oligo directed mutagenesis. In house cloning vectors, designated as pENDs, was modified by two undergraduate students to remove redundant EcoRV DNA restriction sites and to facilitate cloning of the stem-loop mutant oligos. pENDs is a cloning vector. This vector was developed in house in Dr. George Turner's lab. This pENDs vector is customized and termed separately based on the presence or absence of specific restriction sites. The two pENDs vectors which were used to clone the mutant oligomers were pENDs XXI and pENDs VII. pENDs XXI was used to subclone the WT 31, C2A, G11C, G11A and T6C

mutant oligomers. pENDS VII was used to subclone G8A, AI0C, M8, M10 and M14 mutant oligomers.

The cloning vector pENDS links the coding region of GPCR to *bop* gene transcription and translation control elements (34). The pENDS vector also includes the carboxyl-terminal coding sequence which contains two short peptide sequences, one being the six consecutive histidines and the other being an epitope from Influenza Hemagglutinin protein (HA). These short peptide sequences or "tags" can facilitate immunological detection and purification of the receptor protein (46). The DNA fragments from the pENDS vectors can be transferred into *Hsalinarum* expression vectors [designated pHex, for Halobacterium expression vectors (34, 47)].

B. Subcloning into expression vector (pHex)

Hsalinarum expression vector (pHex) is based on pUBP2 which is a shuttle vector for *E.coli* and haloarchaeal organisms. (34, 48-50). pHex can be termed as a shuttle vector because it possesses replicons which are derived from both *E.coli* and *Hsalinarum*. pHex also possesses genes which confer resistance to both ampicillin and mevinolin (an HMG-CoA reductase inhibitor (51)) for host *E.coli* and *Hsal*, respectively. Hence pHex vector can be expressed in both *E.coli* and *Hsal*. The pHex vector containing the mutant oligomer can be expressed in the *Hsal*. The pHex is expressed in a bR negative strain of L33. Under normal conditions and in the absence of Mevinolin, L33 colonies are white in color due to the absence of bR producing molecular machinery. L33 cannot survive in the presence of 10 μ M Mevinolin (Mev) i.e without the pHex the L33 will not form any colonies on a Mev plate. The presence of the pHex vector with the mutant oligomer induces Mev resistance in L33 and also forms colonies. The color of the

colonies depends on the mutant oligomer nucleotide interaction and the probable stability of the stem loop structure. Further, the colony color provides a visual assay for bR expression. The colonies can be later isolated for bR quantification, mRNA analysis and other types of assays.

The cloning vector, pENDs, and expression vector, pHex, are shown in Figure 4.

Figure 5 shows an analytical digest of the two vectors using restriction enzymes

PstI and *BamHI*.

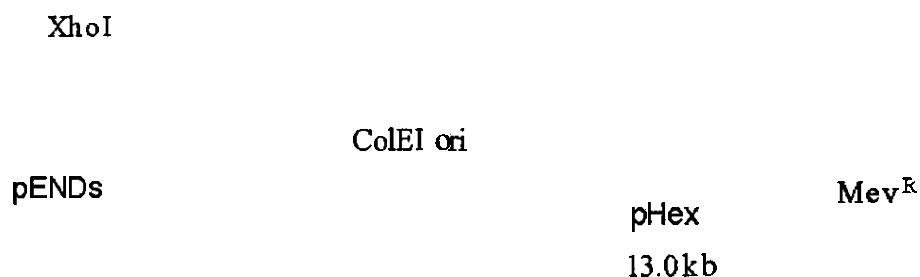


Figure 4 : The cloning vector, pENDS, 3.9 kb and the expression vector pHex, 13.0 kb.

The pENDS vector has an ampicillin resistance marker and a ColE I origin of replication. The halobacterial plasmid pHex has HH9 origin of replication, ampicillin resistance and Mevinolin resistance marker. Mevinolin resistance is encoded by an up-promoter mutation of the HMG-CoA reductase gene. The PstI- BAM HI fragment from the pENDS is ligated into the pHex vector. (47)

pHex and pENDs Analytical Digest

Figure 4 : The pHex and pENDs analytical digest.

The 13.0 kb uncut pHex (1), the 3.9 kb uncut pENDS fragment (3), the 1.2 kb *Pst*I and *Bam*HI fragment which separated from the cut pHex fragment, 11.8 kb remaining (2) or the pENDS, 2.7 kb remaining (4)

Materials and Methods

Bacterial strains

E. coli K12 strains were HB101 derivative D12 z 10 (*leuB6*, *proA2*, *recA13*, *lacY1*, *ara14*, *galK2*, *xyl5*, *mtl1*, *rpsL20*, *supE44*, *hsdS20*, *lacIq*, 12, F2; 39) and DH5a (F2, *recA1*, *endA1*, *gyrA96*, *thi-1*, *hsdRI7* (*r2k*, *mlk*), *supE44*, 12). *H. salinarum* strains were ET1001 (*Vac2*, *BR111*, *Rub2*; 40) and L33 (*Vac2*, *BR2*, *Rub2*; 41).

Media and Growth Conditions

All salts and chemicals were reagent grade from standard biochemical supply houses. Bacteriological peptone was from Oxoid (Unipath LTD., Hampshire, England); yeast extract tryptone, Difeo peptone, and bacto-agar were from Difeo Laboratories (Detroit, MI). Complex *E. coli* medium was yeast extract tryptone. Mevinolin (mev) was a gift from A.W. Alberts; Merck, Sharp, and Dohme, Rathaway, NJ.

Molecular Reagents

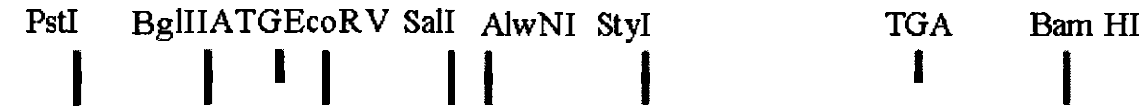
T4 DNA ligase and various restriction endonucleases were purchased from New England Biolabs (Beverly, MA) or from Boehringer Mannheim (Indianapolis, IN). DNA sequencing was done at ACGT, Inc. (Wheeling, IL). Electrophoresis grade agarose was from FMC Corporation (Rockland, ME). Custom oligo-deoxynucleotide primers were purchased from Oligomer OY (Helsinki, FI). Oligo-directed mutagenesis was performed with the QuikChange II Site-Directed Mutagenesis Kit (Stratagene, La Jolla, CA). Molecular Weight Marker is DNA Molecular Weight Marker X, (0.07–12.2 kbp) (Roche, Germany)

Cloning the mutant oligomers into the cloning vector

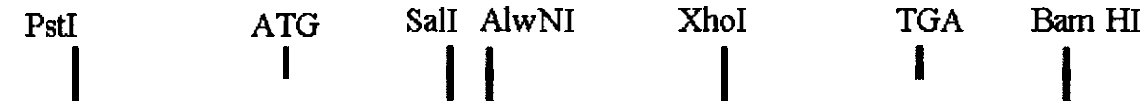
The vector with *BglII*, *EcoRV*, *SalI*, *AlwNI* and *styI* restriction sites within its *PstI*-*BAMHI* fragment was called pENDs XXI. Similarly the vector with *BglII*, *EcoRV*, *SalI*, *AlwNI* and *XhoI* restriction sites within its *PstI*-*BAMHI* fragment was called pENDs XXXI, and the vector with *SalI* and *AlwNI* sites within its *PstI*-*BAMHI* fragment was called pENDs VII. As mentioned above the mutant oligomers were cloned into the two different pENDs vector background.

A. Mutants with pENDS XXI as template for oligo directed mutagenesis.

Oligo directed mutagenesis was used to engineer a silent *StyI* site into the pENDS vector XXI. The vector was sequenced, and the initial sequencing of these mutant oligomers (i.e WT 31, C2A, G11C, G11A and T6C) gave a probable mismatch in the nucleotide sequences downstream of the *SalI* site. Hence the *SalI*-*BamHI* site of the pENDS XXI was removed and subcloned with the *SalI* – *BamHI* site of another pENDS vector (pENDS XXXI). The pENDS XXXI has an *XhoI* site downstream of the *SalI* site unlike the pENDS XXI, which had a *StyI* site downstream of the *SalI* site (Figure 5). Hence a positive sub-cloning would have an *XhoI* instead of *StyI*. This difference was used to identify the sub-clones with restriction digests (Figure 5). Also, the location of the start codon (ATG) was shown relative to the other restriction sites in the *PstI*-*BAMHI* fragment of the pENDs vector.



pENDS XXXI (PstI BamHI fragment)



Subcloned mutants (PstI BamHI fragment)

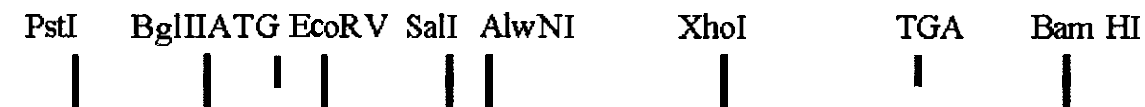


Figure 5: The PstI- BAMHI fragment showing the restriction sites of pENDS vector. The ATG is the start codon and represents the relative location of the stem-loop within the pENDS vector. Mutants C2A, G11C, G11A and T6C had pENDS XXXI as template after the final sub-cloning and hence were compared with wild type pENDS XXXI for all the bR results.

B. Mutants with pENDS VII as template for oligo directed mutagenesis

Oligo directed mutagenesis was also used to engineer a silent *StyI* site into the pENDS VII vector. The pENDS VII vector contained the *SalI* and *AlwNI* sites and positive transformants had both the *SalI* and *AlwNI* sites (Figure 6).

pENDS VII (PstI BamHI fragment)



Figure 6: The *PstI* and *BamHI* fragment of the pENDS VII vector showing the restriction sites. The ATG is the start codon and represents the relative location of the stem-loop within the pENDS vector.

Once these restriction sites were checked the isolation of the 5' *bop* gene in pENDs was done using a preparative restriction digest of 5 µg DNA in 40 µL of NEB or BamHI buffer and 4 µL of 10x BSA incubated at 37°C for 4 hours with 5 µl each of PstI and BamHI restriction enzymes. Total volume of 400 µL was achieved by dilution with nuclease free water.

The digested samples were then loaded onto a preparative agarose gel using 1% agarose dyed with 0.5 µg/mL ethidium bromide. The 1.2 kb fragments containing the 5' *bop* DNA was isolated from the gel and extracted using the Nucleospin® Extact II (Macherey-Nagel Gutenberg, FR) DNA extraction kit. The purified fragments were ligated into the *PstI* and *BamHI* digested pHex vector.

The 1.2 kb *PstI*-*BamHI* fragment from the pENDS, containing the 5'*bop* gene, was subcloned into the *PstI* and *BamHI* digested pHex. The pHex shuttle vector was prepared using the *PstI/BamHI* restriction digest of the pHex vector as described above, and the 11.8 kb (13.0 kb pHex – 1.2kb fragment) was isolated instead of the 1.2 kb dropout fragment.

Once isolated, concentrations of DNA fragments were analyzed using UV-Vis spectrophotometry, and ligation into pHex was performed. Approximately 60-70 ng of insert DNA was incubated with 100 ng of pHex shuttle vector in water, 10X buffer and ligase enzyme (total volume= 20 µL) at 16 °C overnight using a programmable thermo controller.

The following day, 10 µL of the above ligation was incubated with 200 µL of competent cells on ice for 30 min. Samples were heat shocked at 42 °C for 90 sec and then placed back on ice, and 800 µL of pre-warmed SOC was added and incubated at 37

°C for 1 hour on a shaker. A volume of 150 µL of this culture was plated on agar plates with ampicillin. These plates were incubated at 37 °C overnight. Single colonies were isolated by subplating the following day. A single colony was then inoculated into 5 mL culture of LB broth with ampicillin and grown overnight. This culture was pelleted and the pHex DNA was isolated using Promega Wizard® Plus SV Minipreps DNA Purification System. The DNA concentrations were determined using UV- Vis spectrophotometry.

Positive clones were confirmed by restriction digestion with *PstI* and *BamHI* (see Results). Once confirmed the pHEX vector was transformed into *H.sal* under soap free conditions.

Halo Transformation

L33 is the bR negative strain of *H.sal* and hence was used for transformations. The L33 without the vector will not survive under Mev. The presence of the pHex vector, (which contains the Mev resistance marker) allowed L33 to survive in the presence of Mev. L33 was cultured in soap free Yeast extract media (YET–Annexure I). It was important that the cultures and glassware are soap free. Soap disrupts the L33 membrane and would have caused a significantly lower (sometime zero) transformation. The L33 stock was first inoculated into 5 mL of YET and allowed to grow until the culture reaches $OD_{660} \sim 0.4$. This was sub-cultured twice in 5 mL YET (when the culture reaches $OD_{660} \sim 0.4$). This subculture was used to inoculate 50 mL YET media in a conical flask at a final OD_{660} of 0.01. The 50 mL culture seeded with $OD_{660} \sim 0.01$ was allowed to grow until it reaches log phase, and then it was harvested at $OD_{660} \sim 0.4$ (0.2 – 0.6). The cultures are grown at 37 °C in a shaker with 225 rpm. Once the L33 culture reached

OD₆₆₀ ~ 0.4, the conical flask can be removed from the shaker and can be left at room temperature for approximately one week to ten days. This prevented further growth of L33, and the culture could be used for transformation within one week.

The 50 mL culture thus obtained can be used for the polyethylene glycol (PEG) mediated transformation of the pHex vector. Using a clean pipette, 10 mL of the above 50 mL culture was transferred into a round bottom falcon tube, and the cells were pelleted using a SS34 rotor at 3000 rpm for 10 min at room temperature. The media was aspirated while taking care that the pellet was not disturbed. The inside of the tube was dried using applicator sticks, and Kimwipes removed any residual media. The cell pellet was gently resuspended in 1 mL of SS (Annexure I).

A clean 15 mL round bottom falcon tube was taken, and 15 µL of SS EDTA (Annexure I) was added to the bottom of it. Then 200 µL of the above cell suspension (L33 cells resuspended in 1 mL of SS) was added to one side of the falcon tube and mixed with the already added SS EDTA. This mixture was incubated for 30 – 60 seconds. In a clean 1.5 mL eppendorftube, 15 µL of SS solution was added and 1µg of the DNA (which was extracted from the *E.coli*) was resuspended in this 15 µL of SS solution. From this eppendorftube (which contains 15 µL of SS solution and 1µg of the DNA), 10 µL of the DNA suspension was taken and added to the 15µL SS EDTA + 200 µL cell suspension solution and incubated at room temperature for 5 min. After 5 min, 235 µL (equal to 200 µL cell suspension+ 15 µL SS EDTA + 10 µL DNA) of 60% w/v Polyethylene glycol (PEG) was added to the round bottom falcon tube (52). In order to prepare 60% w/v PEG, 3.0 grams of PEG was dissolved in 5 mL of SS solution. The total volume in the round bottom falcon tube was 470 µL (200 µL cell suspension+ 15 µL SS

EDTA + 10 μ L DNA+ 235 μ L PEG) This 470 μ L of solution was mixed very gently by inversion 20 times and incubate at room temperature for 20 min. Following the incubation, 5-7 mL SDS (Spheroplast Diluting solution) (Annexure I) was added gently to the round bottom falcon tube and incubated at 42°C for 2-4 hrs without agitation. After 2-4 hrs the cells were pelleted in a SS34 rotor at room temperature at 5000 rpm for 20 minutes. The supernatant was aspirated and 10 mL of SDS RHM (Annexure I) was added and incubated overnight at 37 °C on a shaker. The following day 5 mL of the culture was pelleted and resuspended in 100 μ l of RHM (with 10 μ M Mevinolin).

Using this 100 μ l cell re-suspension, 1 μ L and 10 μ L of the cell suspension was used to plate two separate 25 μ M mevinolin plates. The plates were incubated at 42 °C. The phenotypes were observed in 15- 20 days. (see Results)

***H.salinarum* expression**

Successful transformation of L33 yielded colonies on the Mev plates because of the presence of the pHex vector. These colonies had different phenotypes based on the mutant oligomers within the pHex vector. The image of the colonies was taken using a Kodak digital camera and integrated density analysis was conducted on the image to determine the intensity of the purple color in the colonies. Since each of the mutants perturbed the stem-loop in a unique way, the colonies had different intensities of purple membrane.

***H.Salinarum* growth and harvest**

After observing the phenotypes in the *H.sal* strain L33 (bop-), the colonies were picked and five of the eleven mutants were cultured to 1 L under Mevinolin. Briefly, each of the mutant and wild type were first inoculated in 5 mL of the Rich Halo Media (RHM

with 10 μ M Mevinolin) (Annexure I) and sub-cultured twice at $OD_{660} \sim 0.6$. A 50 mL solution of RHM (with 10 μ M Mevinolin) was inoculated at a final OD_{660} of 0.1 with these 5 mL cultures and allowed to grow until it reached log phase (i.e $OD_{660} \sim 0.6$). The cells were then spun down at 8000 rpm using a SS34 rotor, and the plasmid DNA was extracted using SV miniprep. A 250 mL solution of RHM (non selective) was inoculated from this 50 mL culture. The remaining 50mL culture was used for plasmid DNA extraction. The 250 mL culture was allowed to grow until $OD_{660} \sim 0.6$. It was then used to establish 1 L nonselective cultures in 3-L Fernbach flasks. This 1 L culture was used for growth curve and bR quantifications (32).

Growth curve and bR quantification

Five mutants were chosen for bR quantification. For the purpose of uniformity, all the mutants with pENDS XIII as final background for subcloning (WT, C2A, G11A, G11C and T6C) were grown up to 1 L cultures and used for bR quantification. The 1 L cultures were allowed to grow from inoculation ($OD_{660} \sim 0.01$) to stationary phase ($OD_{660} 1.0 \sim 3.0$). At approximately every 12 hrs, the OD_{660} reading was taken for each of the five mutants. Simultaneously, 40 mL of the culture was collected at every 12 hrs and centrifuged at 3000 rpm using SA 600 rotor for 30 min. The pellet was transferred to a 1.5 mL centrifuge tube and centrifuged at 6000 rpm for 5 min. The supernatant was removed and the pellet stored at $\sim 80^{\circ}\text{C}$ for mRNA analysis. In the future these samples can be used for mRNA analysis.

Once each of the cultures reached stationary phase, the cells in the remaining culture were pelleted at 5000 rpm and resuspended in 30 mL of RHM (annexure I). The whole cells were washed (in basal salt – annexure I), and bR values were obtained by

taking OD~568. bR accumulation was normalized to equivalent number of cells for comparative analysis. (53)

Transformation back into *E.coli*

In order to double check the pHex vector transformation process into the *H.sal*, the vector was transformed back into *E.coli*. The transformation into *E.coli* also gave a chance to extract vector DNA in quantities necessary for sequencing and further assays. *E.coli* had higher plasmid number per transformant than *H.sal* for the same pHex vector, and hence it was logical to use *E.coli* for producing the vector DNA fragment for further analysis. The plasmid DNA from *Hsal* was extracted using the miniprep. The plasmid DNA obtained from miniprep was transformed back into *E.coli* using the heatshock method. The DNA from the resulting transformants was extracted and checked for the *PstI* and *BamHI* fragment by restriction digest. Since all the mutants and the wild type had the *PstI-BamHI* fragment (see Results), these DNA samples were sent for sequencing (ACGT, Inc. Wheeling, IL). The DNA sequence confirmed the presence of the original stem loop in all the mutants except T6C.

Mfold predictions for the wild type and the mutants

In silico secondary structure predictions (mfold) indicated the presence of cooperative base pairing interactions between the nucleotides within the stem loop structure. Mfold is a predictive algorithm which has proven useful for predicting the secondary structure of a single stranded nucleic acid. The simulation of the folding can be done under various salt concentrations. The portal for the mfold web server is <http://www.bioinfo.rpi.edu/applications/mfold>. The lower the ΔG value the stronger

would be the base pairing and hence an increased stability in the stem loop secondary structure.

Twenty five nucleotides representing the stem loop structure were used for the mfold analysis(54) under the following set conditions:

- The DNA sequence is linear.
- Folding temperature is set to 37°C
- Ionic conditions: $[\text{Na}^+] = 1.0 \text{ M}$.
- Standard errors are roughly $\pm 5\%$, $\pm 10\%$, $\pm 11\%$ and 2-4 °C for free energy, enthalpy, entropy and T_m , respectively.

Integrated density analysis:

The colonies that were observed were photographed, and integrated density analysis was done using imageJ software.

Results

I. Mfold predictions

Mfold program predicted the different structures which might be formed due to the nucleotide interactions of the stem-loop oligo-nucleotides (Annexure II). Several mutants had more than one predicted structure (Table 1). These structures had differing ΔG values indicative of their stability: the lower the value the more stable the secondary structure. Mfold predicted two possible structures for the wild type oligonucleotide sequence. The wild type structure with ΔG value of -4.14 (structure 1) has a more stable base pair interaction within the stem loop than the structure with ΔG value of -3.20 (structure 2). In order to understand which of the two structures actually exists in the wild type, the mutant C2A was used. C2A mimicked structure 1 of the wild type. The results showed that the C2A mutant had significantly different Integrated Density and bR than that of the WT, thereby indicating that the stem loop of WT might take the structure 2 configuration. This can be further investigated using comparative mRNA analysis of C2A and WT31.

Table1 : ΔG & T_m values calculated for WT and mutants using Mfold. WT= Wild Type, DM = double mutant (T6C:G8C), TM= Triple Mutant (T6C:G8C:A20C)

Mutant	Structure1 ΔG	Structure2 ΔG	Structure3 ΔG	Structure4 ΔG	Structure5 ΔG	Average of ΔG	T_m Values
WT	-4.14	-3.20				-3.67	59.50
C2A	-4.14					-4.14	65.30
T6C	-1.98					-1.98	55.50
G8A	-0.35	-0.25	-0.24	0.10		-0.19	39.50
A10C	-7.05	-6.11				-6.58	71.80
G11A	-4.14	-3.20				-3.67	59.50
G11C	-4.14	-3.20				-3.67	59.50
A14G	-4.14	-3.20				-3.67	59.50
DM	-0.35	-0.24	0.10	0.18	0.24	-0.01	37.56
TM	-0.35	0.10	0.24	0.37		0.09	36.18

The ΔG value for each mutant was calculated using Mfold (Table 1) and shown in Figure 7. Mfold analysis predicted a single structure for T6C with a ΔG of -1.98 . A higher ΔG value indicated that the stem loop is destabilized. The predicted average ΔG values of G8A, DM and TM ranged from -0.19 to 0.09 and were more than that of the wild type (-4.14 and -3.67). This indicated weaker base pairing among the stem loop nucleotides. The predicted average ΔG value of G11A, G11C and A14G were all -3.67 and therefore similar to that of the Wild type (-3.67). Mutant C2A had an average ΔG value (-4.14) lower than that of the Wild type (-3.67) and hence showed stronger base pairing in the stem-loop. Mutant A10C had a significantly smaller ΔG value (-6.58) and hence had the strongest base pairing among all the mutants. The predicted stem-loop structures of each of the mutants along with their thermodynamics are shown in Annexure II. It was observed for A10C that there was probably non base-pair interaction between G (eleventh position) and T (sixteenth position), which may have accounted for its greater stability (Annexure II). This could be attributed to the additional hydrogen bonding in the stem region of the stem-loop.

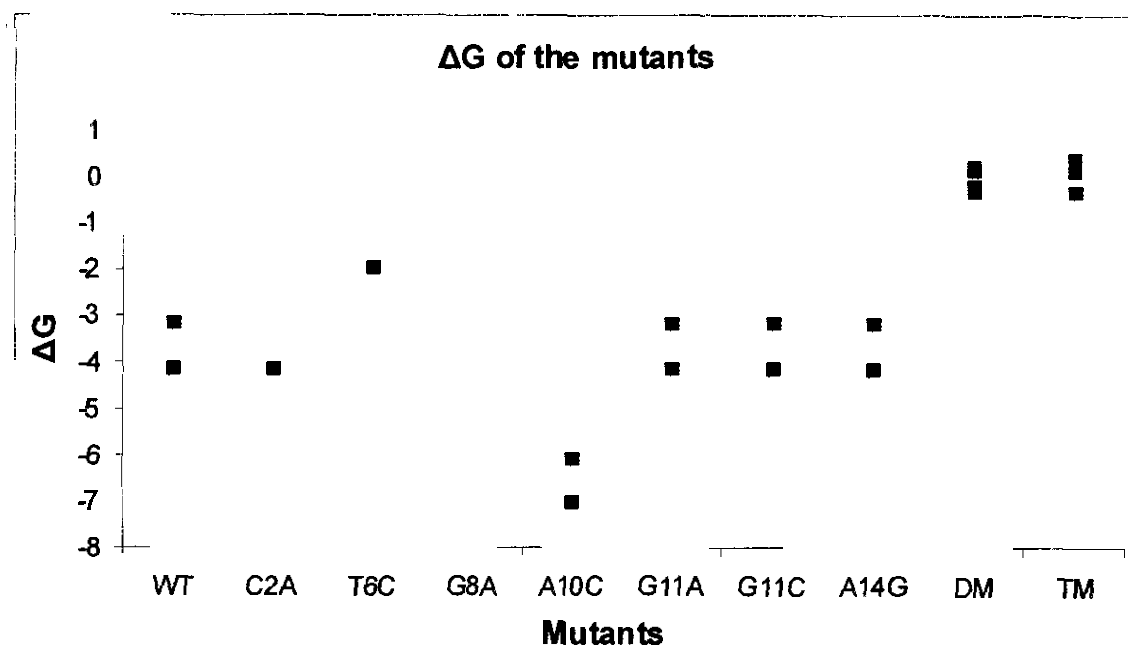


Figure 7: ΔG values of different mutants calculated using M-fold algorithm. (N = 1 to 5)

II. Sub-cloning into pENDS vector.

A. Mutants with pENDS XXI as template for oligo directed mutagenesis.

The WT XXXI and the mutants C2A, G11C, G11A and T6C were checked for *XhoI*, *ECORV*, *Bgl II* and *StyI* sites. The colonies which had a *StyI* site instead of a *XhoI* were shown as negative in the Figure 8 below. A positive sub-clone had *XhoI*, *ECORV* and *Bgl II* restriction sites. Mutants C2A, G11C, G11A and T6C had pENDS XXXI as template after the final sub-cloning and hence were compared with wild type pENDS XXXI for all the bR and integrated density results.

Negative

Wild Type

Figure 8: Restriction digests of pENDs vector (pENDS XXXI)

Top lane: Negative (pENDS XXI vector) and WT31. Bottom lane: G11A, G11C, T6C and C2A. Lane 1: pENDS undigested, Lane 2: pENDs digested with *styI*, Lane 3: pENDs digested with *xhoI*, Lane 4: pENDs digested with *EcoRV*, Lane 5: pENDs digested with *BglII*.

B. Mutants with pENDS VII as template for oligo directed mutagenesis

Mutants G8A, A10C, G8A, A10C and A14G had pENDS VII as template for oligo directed mutagenesis. After the sub-cloning the mutants were checked for *Sall* and *AlwNI* restriction sites (Figure 9). The mutants had *Sall* and *AlwNI* restriction sites. These mutants were compared with wild type pENDs VII for the integrated density results.

Figure 9: A Representative result of all gels with pENDs VII as template for oligo directed mutagenesis. Lane 1: pENDS undigested, Lane 2: pENDs digested with *Sall*, Lane 3: pENDs digested with *AlwNI* Lane 4: pENDs digested with *XhoI*. Mutants G8A, A10C, M8, M10 and M14 had pENDS VII as template for oligo directed mutagenesis and hence were compared with wild Type VII for the integrated density results.

Isolating the *PstI*-*BAMHI* fragment of the pENDS vector

After the restriction sites of the mutants were confirmed, the *PstI*- *BAMHI* fragment of the pENDS vector (of all the mutants) were isolated. A representative gel image of the *PstI*- *BAMHI* drop down fragment is shown in Figure 10 below. The mutants shown in the gel image were *G11A* and *G11C*.

3.9kb
2.7kb

1.2kb

Figure 10: Representative gel showing the digest of the *PstI* and *BamHI* fragment. The digests of mutants *G11A* and *G11C* with *PstI* and *BamHI* are shown. The gel image before (left) and after (right) the fragment was excised out. The 3.9 kb uncut pENDS fragment digested into the 1.2kb *PstI* and *BamHI* fragment and the 2.7kb fragment.

The 1.2 kb *PstI*-*BamHI* fragment from the pENDS was successfully ligated with *PstI* and *BamHI* digested pHex. The vector was further checked for the presence of the *PstI* and *BamHI* fragment by restriction digest before transformation into the *H.salinarum* (Figure 11).

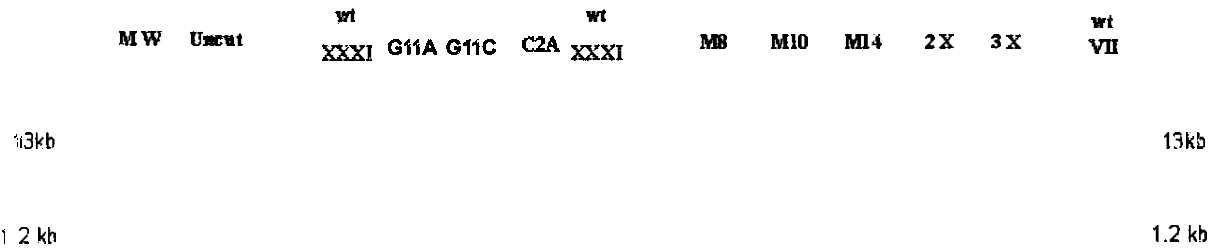


Figure 11: *PstI - BamHI* fragment before transformation into *Halobacterium salinarum*. The molecular weight marker (MW), Uncut pHex fragment (uncut) and the 1.2kb *PstI* and *BamHI* drop out fragment of the mutants.

Transformation back into *E.coli*

The transformation into *Hsalinarum* was under soap free conditions, the colonies were observed in 15 to 20 days (Figure 13). The colonies were grown selectively and the plasmid DNA was extracted and transformed back into *E.coli*. Successful transformants were isolated and the plasmid DNA from the *E.coli* was extracted. Restriction digest for *PstI - BamHI* (Figure 12) was done on this plasmid DNA to check for accuracy of the transformation. The plasmid DNA was sent for DNA sequencing.

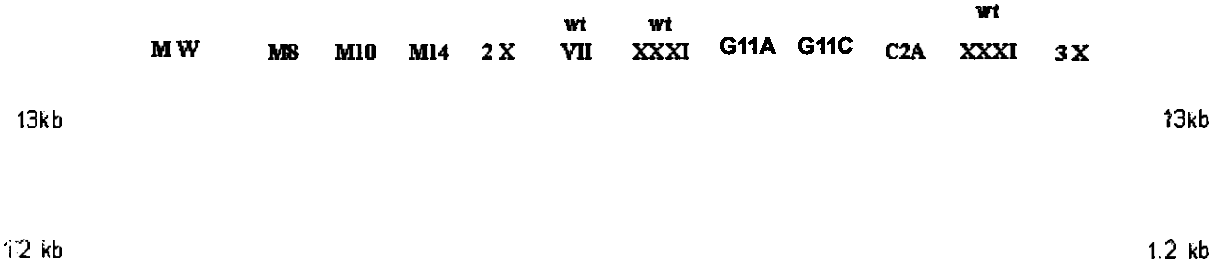


Figure 12 : *Pst I - BAM HI* digest of the plasmid DNA from *E.coli* The Molecular weight Marker, Uncut pHex fragment and the 1.2kb *PstI* and *BamHI* drop out fragment of the mutants.

DNA sequencing

DNA sequencing confirmed the presence of the mutant oligomer sequence in all the mutants except T6C. It was noticed that T6C had exactly the same sequence as that of WT XXXI. The sequence of T6C mutant was exactly the same as that of the wild-type right from the initial sub-cloning into pENDs vector. Hence the bR quantification and integrated density values of this mutant were considered as WT and an average value was used for subsequent calculations. WT31 might have been accidentally used instead of T6C during the initial ligation of the T6C mutant oligomer into the *Pst I - BAM HI* fragment and hence the error might have occurred.

III. Integrated Density Analysis.

The colony image was used to calculate the integrated density (Figure 13). This gave an estimate of the purple pigmentation and thereby the level of *bop* gene expression. The integrated density analyses of the mutants indicated that A10C had the least integrated density, i.e the colonies were the least purple in color (Figure 14).

Figure 13: Colony image of the mutants transformed into L33: The colonies for A10C were white, where as the remaining colonies of other mutants had different intensities of purple.

The A10C colonies appeared white to the naked eye. The lack of bR accumulation was consistent with having the lowest average ΔG (calculated using Mfold) among the mutant oligomers. C2A and A10C should have increased the stability of the stem-loop, and hence, this might have caused the decrease in the bR accumulation. Since C2A had significantly lower integrated density and bR values than WT, the stem-loop structure for WT was not that of C2A as indicated by Mfold analysis (Table 1, Figure 7). The integrated density of the other mutants DM, A14G, G8A TM and G11C were also less than the Wild type. WT expressed maximum integrated density and hence the most purple colonies. The integrated density gave a rough estimate of the intensity of the purple color and was a very crude method of estimating the levels of bR. In order to obtain more accurate bR quantifications, further studies like mRNA quantification, bR isolation and measurements using sucrose gradient are needed.

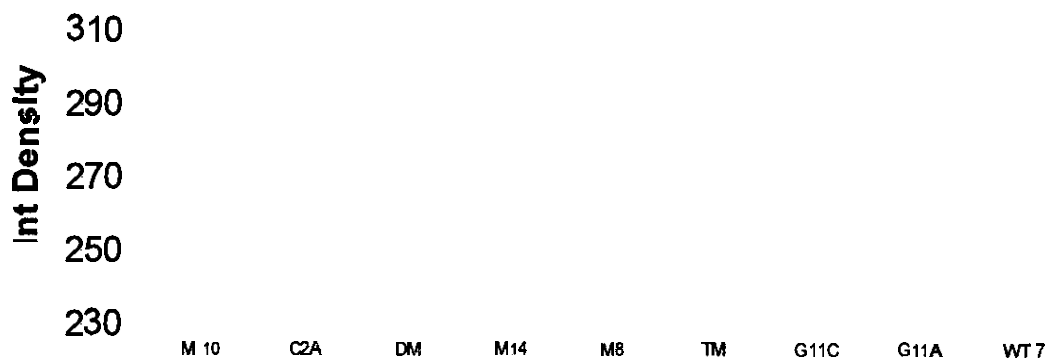


Figure 14: Integrated density values of the colony images calculated using imageJ software. (N = 1)

IV. Growth curves

The growth curves indicated that the cells had some lag phase before they entered into the log phase. In about 150 hrs, the cells reached stationery phase and were harvested for bR quantification (Figure 15). The growth curves were used to observe the growth of the various mutants over a period of time. bR accumulation was maximum in the stationery phase (53), and hence these growth curves helped to decide the correct time for bR harvest.

Growth Curves

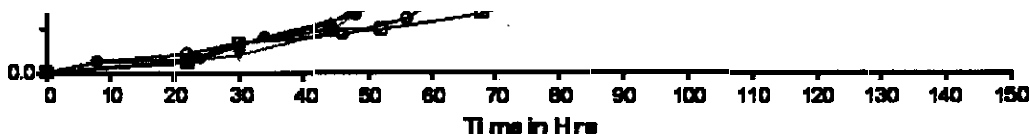


Figure 15: Growth curves of the mutants: The absorbance at OD 660 (Y-axis) was plotted against time (X axis).

Once the cells reached stationery phase, the cells were harvested from the cell culture. The culture T6C took more time than other cultures to reach log and stationery phase. The main objective of using this growth curves was to make sure the cultures reach stationery phase before they were harvested.

V. bR quantification

bR quantification was done for each of five mutants: WTXXXI, C2A, G11A and G11C. Since the T6C mutant had a wild type DNA sequence, its bR value was averaged with the WT XXXI. The C2A had the least amount of bR accumulation (72%). WT XXXI had the highest amount of bR. G11A (85.5%) and G11C (79.4) had less accumulation of bR than WT, but more than that of C2A. The bR results indicated that the WT *bop* gene had a structure which may not be similar to that of C2A. (Figure 13).

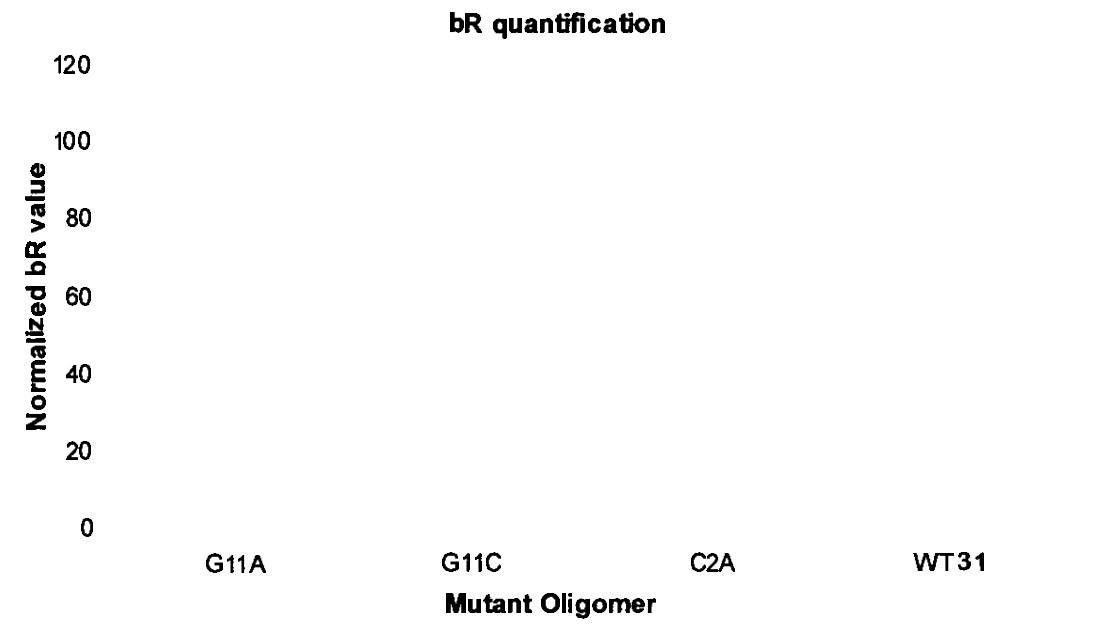


Figure 16: bR quantification of the mutants G11A, G11C and C2A in comparison with the wild type XXXI. (WT 31 = Wild type XXXI). The OD values are taken at 568 nm. For normalizing: The WT which has the maximum bR value is set to 100 and the bR for the remaining mutants are calculated as percentage. The bR value of WT is an average of WT31 and T6C. (N = 1)

The results obtained by bR quantification were in-line with those obtained using integrated density analysis.

Discussion:

bR is the sole membrane protein produced by the bacterio-opsin gene (*bop*) (21), hence bR quantification was used to understand the *bop* gene transcription and translation efficiency of the mutants. Earlier studies have established the requirement of the TATA box and UAS for *bop* promoter activity (38). The putative stem-loop structure within the *bop* gene mRNA is considered to be a key component of the molecular machinery which regulates Bop synthesis and it is important to maintain the *bop* mRNA stem-loop structure to produce Bop (55).

In the study presented here, the mutant oligomers were successfully expressed *in-vivo* using the in-house cloning and expression vectors (pENDs and pHex); the bR quantification and integrated density analysis of these mutants indicated that there were noticeable differences among the bR accumulation in these mutants (Figure 14, 16). The differences could be attributed to the stem-loop perturbations. These perturbations might be associated with mRNA degradation rate and /or ribosomal binding. Hence, it can be concluded that the putative stem loop structure indeed exists *in-vivo* within the plasmid expression system that we have been trying to develop.

Further, using the Mfold analysis, it could be understood that any perturbation in the nucleotides of the stem-loop had a corresponding change in the ΔG values (Table 1, Figure 7). Destabilizing the chain was predicted to increase the ΔG (54). The mutant oligomers, which were expected to increase the stability of the stem-loop structure (based on mfold analysis), did show the lower integrated densities. For example, A10C had the lowest ΔG (-6.58) and also had the lowest integrated density (Figure 14). The associated colonies of A10C were white. Similarly C2A, which had the second lowest ΔG value

amongst the mutants ($\Delta G -4.14$) had the second lowest integrated density (Figure 14). Based on the results above, the utility of the M-fold study was established for *H.sal* such that any increase in the stability of the stem loop corresponded with a decrease in the integrated density of the colonies.

Further, the bR and integrated density values of these mutants indicated that any perturbation to the wild type stem-loop structure was associated with decreases in the bR accumulations (Figure 14, 16). Taken together, the data supported the hypothesis that the bacterio-opsin gene has been highly optimized to achieve maximal levels of bR accumulation. Previous research by other labs have also indicated that single base pair substitutions in the stem-loop region significantly reduce the protein expression (56).

The nucleotide interaction in the stem-loops of each of the mutants helped to understand the cis-acting determinants of the stem-loop structure. For example, the structure of C2A ($\Delta G -4.14$) had a lower average ΔG value compared to Wild type ($\Delta G -3.67$). The Mfold analysis of the Wild type mutant indicated two probable structures, one with $\Delta G-4.14$ and the other with $\Delta G-3.67$. C2A was expected to mimic the $\Delta G -4.14$ structure of the wildtype (structure 1 –Annexure II) as per the Mfold prediction. However, the bR and integrated density values of C2A were significantly different from that of the Wild type (Figure 14, 16), hence the WT stem-loop might have a secondary structure which is distinct from that of C2A and might take the structure 2 shown in the annexure II below. Also the results indicated a minor role for the SD#1 element. G8A, A10C, G11A, G11C, DM (T6C:G8C) and the TM (T6C:G8C:A20C) perturb the SD#1 of the stem-loop. However, the decrease in the bR was not very significant compared to A14G, which did not perturb the SD#1. Scanning mutagenesis within the mRNA leader

of another gene, *gvp* gene, (which are involved in gas vesicle formation in *H.sal*) demonstrated that mutations adjacent to the putative SD sites in the *gvp* gene did not influence the efficiency of translation in *H.sal*.(57). In some archaeas the open reading frames can be translated *in-vitro* using either SD dependent pathway or leaderless pathway. (58). The bioinformatics genome analysis of archaea reveal that less than 10% of the genes contain SD sequence (59). Hence, it can be concluded with reasonable confidence that SD#1 might play a minor role in the bR accumulation; however, a more quantitative method like mRNA analysis would probably help better understand the differences.

Further, for the mutant A10C, it should be noted that the mutation of Cytosine (C) with Adenosine (A) at the tenth location in A10C could have caused the resultant mRNA to code for GAG (Glutamic acid) instead of GCG (Alanine). This was the only mutant (other than G11C) which caused the mRNA to translate a different amino acid than that of the Wild type. Glutamic acid is an acidic aminoacid, and alanine is a non-polar amino acid. The different amino acid might have resulted in the decreased bR accumulation and hence the decreased integrated density values. This mutant also perturbs the SD#1 site, hence additional studies using different mutants would be required to tweak apart the actual reason for the decrease in the bR accumulation in mutant A10C.

Summary

An expression system like *H.sal* might provide a platform for the over expression of transmembrane proteins which are homologous to bR. In order to exploit the molecular machinery of *H.sal*, it is imperative to first understand the biology of this Archaea. Further, it is well established that there is very strong coupling between translation and mRNA stability in *H.sal* (60). In pursuit of this, our lab has previously generalized and simplified the *H.sal* system by creating convenient cloning sites within the *bop* gene. Our lab has also established the factors which stabilize the plasmid directed membrane protein expression i.e the heterologous gene transcription and/or translation products. Our lab has also tagged the *bop* gene by introducing specific sequences, which enables purification and identification of the protein (47). Further, we are trying to understand the various facets of the *bop* gene expression.

We understand that the N-terminal part of the *bop* gene has numerous determinants of expression (29, 39), and in continuation with our pursuit to understand the molecular mechanism, the above study was conducted targeting especially the stem-loop structure at the 5' end of the *bop* gene. The study presented herein adds to the existing science about the molecular biology of the host organism *H. sal* especially in relation to the 5' end of the *bop* gene stem-loop structure. Although, other labs have also used strategies similar to our lab to express homologous halorhodopsin and sensory rhodopsin (24, 61-64), currently their transgenic expression of membrane protein (both *in vitro* and *in vivo*) has had minimal results (65, 66). The occurrence of high density membrane in *H.sal* and its scope for expression of other GPCR is a powerful motivation for continued research on this model system.

The overall findings of this study were as follows:

1. *The bop gene 5' stem-loop structure exists in-vivo:* The mutant oligomers representing the stem-loop structure were expressed in the *H.sal*. A significant difference in the phenotypes of the resultant colonies among the mutants was observed, which indicated that the bop gene stem-loop structure exists *in-vivo* (Figure 13, 14). The bR analysis of the mutants also indicated that there is a significant difference among the mutants (Figure 16). Though the presence of a stem loop like structure was previously established in *H.sal* (60), this finding is new to our plasmids (pENDS and pHex) mediated expression, and opens avenue for future experimentation using the plasmids pENDs and pHex.

ii. *The structure of bop gene 5' stem-loop has a role in the regulation of bacterio-opsin (bop) gene synthesis:* There is a significant difference in the bR accumulation within the mutants (Figure 13, 14 16). It has been previously established that critical determinants of expression resides in the downstream coding region of wild type bop gene (48). It has been previously established that majority of haloarcheal transcripts are leaderless and did not contain SD sequences(59). This work shows that perturbations made to the SD#1 of the stem-loop had no direct significance on the stem-loop structure. Hence the GGAG sequence might not be a proper SD sequence. Further, this work shows that the 5' end of the stem-loop has a role in the regulation of bop gene synthesis. However the regulation of gene expression in Archaea is still a question to be answered.

iii. *With an increase in the stability of the stem loop the bop gene synthesis decreases significantly:* A10C and C2A are the mutants which had an increase in the stability of the bop gene (Refer to ΔG information from Table 1). A10C produced white colonies on

solid media (indicating significant loss of bR accumulation within the cell). bR quantification of C2A indicated that the bR accumulation in C2A is significantly lower than that of the wild type.

iv. *A decrease in the stability of the stem loop was found to only decrease the bop gene synthesis slightly* (Figure 13 14 16). All of the mutants that decreased the stability of the bop gene, i.e. G8A, G11A, G11C, DM and TM, had integrated densities less than that of the WT. The bR quantification of G11C and G11A was also less than that of the wild type 31.

v. *The bacterio-opsin gene has been highly optimized to achieve maximal levels of bR accumulation.* An increase or decrease in the stability of the stem-loop decreases the bop gene accumulation (point iii and iv above). It has been previously established that single base pair substitutions in this region, which did not effect the amino acid caused significant reduction in the protein expression (56). Hence *bop* gene is highly optimized to achieve maximum level of bR accumulation

vi. *Stem-loop and hair pin:* It has also been previously established that the bop mRNA can form a hairpin structure at its 5' end. (29). The presence of a hairpin is required to prevent the rapid degradation of mRNA (56). However, the increase in the stability of the stem-loop structure of the bop gene might cause hindrance to the transcription and translational machinery for the bR synthesis. This can be correlated to similar mRNAs where a secondary structure (hair-pin) causes the decrease or no transcription and translation of the protein. Hence it can be hypothesized that there is indeed the presence of a stem loop structure in the bop gene mRNA.

vii. Future studies should in quantification of purified bR and bop gene mRNA. The integrated density is a crude method to establish the bR accumulation. The bR quantification method used is relatively accurate (53), however a mRNA analysis much more quantitative and accurate to determine the bR accumulation.

Literature Cited

- (1) Wess, J. (1998) Molecular basis of receptor/G-protein-coupling selectivity. *Pharmacol Ther* 80, 231-64.
- (2) Catapano, L. A., and Manji, H. K. (2007) G protein-coupled receptors in major psychiatric disorders. *Biochim Biophys Acta* 1768, 976-93.
- (3) Salazar, N. C., Chen, J., and Rockman, H. A. (2007) Cardiac GPCRs: GPCR signaling in healthy and failing hearts. *Biochim Biophys Acta* 1768, 1006-18.
- (4) Weir, C. J. (2007) *Anaesthesia & Intensive Care Medicine* 8, 437-442.
- (5) McCusker, E. C., Bane, S. E., O'Malley, M.A., and Robinson, A. S. (2007) Heterologous GPCR expression: a bottleneck to obtaining crystal structures. *Biotechnol Prog* 23, 540-7.
- (6) Sarramegna, V., Talmont, F., Demange, P., and Milon, A. (2003) Heterologous expression of G-protein-coupled receptors: comparison of expression systems from the standpoint of large-scale production and purification. *Cell Mol Life Sci* 60, 1529-46.
- (7) Grishammer, R., and Tate, C. G. (2003) *Biochim Biophys Acta* 1, 1610.
- (8) Palczewski, K., Kumasaka, T., Hori, T., Behnke, C. A., Motoshima, H., Fox, B. A., Le Trong, I., Teller, D. C., Okada, T., Stenkamp, R. E., Yamamoto, M., and Miyano, M. (2000) Crystal structure of rhodopsin: A G protein-coupled receptor. *Science* 289, 739-45.
- (9) Okada, T., Fujiyoshi, Y., Silow, M., Navarro, J., Landau, E. M., and Shichida, Y. (2002) Functional role of internal water molecules in rhodopsin revealed by X-ray crystallography. *Proc Natl Acad Sci US A* 99, 5982-7.
- (10) Okada, T., Sugihara, M., Bondar, A. N., Elstner, M., Entel, P., and Buss, V. (2004) The retinal conformation and its environment in rhodopsin in light of a new 2.2 Å crystal structure. *J Mol Biol* 342, 571-83.
- (11) Li, J., Edwards, P. C., Burghammer, M., Villa, C., and Schertler, G. F. (2004) Structure of bovine rhodopsin in a trigonal crystal form. *J Mol Biol* 343, 1409-38.
- (12) Kobilka, B., and Schertler, G. F. (2008) New G-protein-coupled receptor crystal structures: insights and limitations. *Trends Pharmacol Sci* 29, 79-83.
- (13) Baldwin, J.M. (1993) The probable arrangement of the helices in G protein-coupled receptors. *Embo J* 12, 1693-703.
- (14) Baldwin, J.M., Schertler, G. F., and Unger, V. M. (1997) An alpha-carbon template for the transmembrane helices in the rhodopsin family of G-protein-coupled receptors. *J Mol Biol* 272, 144-64.
- (15) Kyte, J., and Doolittle, R. F. (1982) A simple method for displaying the hydropathic character of a protein. *J Mol Biol* 157, 105-32.
- (16) Hjorth, S. A., Schambye, H. T., Greenlee, W. J., and Schwartz, T. W. (1994) Identification of peptide binding residues in the extracellular domains of the AT1 receptor. *J Biol Chem* 269, 30953-9.
- (17) Chen, F., Wang, Y., and Puett, D. (1992) The carboxy-terminal region of the glycoprotein hormone alpha-subunit: contributions to receptor binding and signaling in human chorionic gonadotropin. *Mol Endocrinol* 6, 914-9.

- (18) Ohyama, K., Yamano, Y., Sano, T., Nakagomi, Y., Hamakubo, T., Morishima, I., and Inagami, T. (1995) Disulfide bridges in extracellular domains of angiotensin II receptor type IA. *Regul Pept* 57, 141-7.
- (19) Sofolarides, M. J. (2008) in *Department of Chemistry and Biochemistry*, Seton Hall University.
- (20) Pebay-Peyroula, E., Rummel, G., Rosenbusch, J.P., and Landau, E. M. (1997) X-ray structure of bacteriorhodopsin at 2.5 angstroms from microcrystals grown in lipidic cubic phases. *Science* 277, 1676-81.
- (21) Oesterhelt, D., and Stoeckenius, W. (1974) Isolation of the cell membrane of *Halobacterium halobium* and its fractionation into red and purple membrane. *Methods Enzymol* 31, 667-78.
- (22) Neutze, R., Pebay-Peyroula, E., Edman, K., Royant, A., Navarro, J., and Landau, E. M. (2002) Bacteriorhodopsin: a high-resolution structural view of vectorial proton transport. *Biochim Biophys Acta* 1565, 144-67.
- (23) Oesterhelt, D., and Stoeckenius, W. (1971) Rhodopsin-like protein from the purple membrane of *Halobacterium halobium*. *Nat New Biol* 233, 149-52.
- (24) Krebs, M. P., Hauss, T., Heyn, M. P., RajBhandary, U. L., and Khorana, H. G. (1991) Expression of the bacteriorhodopsin gene in *Halobacterium halobium* using a multicopy plasmid. *Proc Natl Acad Sci USA* 88, 859-63.
- (25) Magyari, K., Balint, Z., Simon, V., and Varo, G. (2006) The photochemical reaction cycle of retinal reconstituted bacteriorhodopsin. *J Photochem Photobiol B* 85, 140-4.
- (26) Mathies, R. A., Brito Cruz, C.H., Pollard, W. T., and Shank, C. V. (1988) Direct observation of the femtosecond excited-state cis-trans isomerization in bacteriorhodopsin. *Science* 240, 777-9.
- (27) Oesterhelt, D., and Stoeckenius, W. (1973) Functions of a new photoreceptor membrane. *Proc Natl Acad Sci USA* 70, 2853-7.
- (28) Turner, G. J. (2008) Mutagenic analysis of membrane protein functional mechanisms: bacteriorhodopsin as a model example. *Methods Cell Biol* 84, 479-515.
- (29) Dunn, R., McCoy, J., Simsek, M., Ajumdar, A., Chang, S. H., Rajbhandary, U. L., and Khorana, H. G. (1981) The bacteriorhodopsin gene. *Proc Natl Acad Sci USA* 78, 6744-8.
- (30) Woese, C.R., and Fox, G. E. (1977) Phylogenetic structure of the prokaryotic domain: the primary kingdoms. *Proc Natl Acad Sci USA* 74, 5088-90.
- (31) Stoeckenius, W., and Rowen, R. (1977) A morphological study of *Halobacterium halobium* and its lysis in media of low salt concentration. *J Cell Biol* 34, 365-93.
- (32) Turner, G. J., Miercke, L. J., Mitra, S. K., Stroud, R. M., Betlach, M. C., and Winter-Vann, A. (1999) Expression, purification, and structural characterization of the bacteriorhodopsin-aspartyl transferase fusion protein. *Protein Expr Purif* 17, 324-38.
- (33) Turner, G. J., Chittiboyina, S., Pohn, L., Hines, K. G., Correia, J. J., and Mitchell, D. C. (2009) The bacteriorhodopsin carboxyl-terminus contributes to proton recruitment and protein stability. *Biochemistry* 48, 1112-22.
- (34) Winter-Vann, A. M. et al. (2001) Perspectives on solid state NMR in Biology. 141-160.

- (35) Schafer, G., Engelhard, M., and Muller, V. (1999) Bioenergetics of the Archaea. *Microbiol Mol Biol Rev* 63, 570-620.
- (36) Olsen, G. J., and Woese, C.R. (1997) Archaeal genomics: an overview. *Cell* 89, 991-4.
- (37) Gropp, F., Gropp, R., and Betlach, M. C. (1995) Effects of upstream deletions on light- and oxygen-regulated bacterio-opsin gene expression in *Halobacterium halobium*. *Mol Microbiol* 16, 357-64.
- (38) Baliga, N. S., and DasSarma, S. (1999) Saturation mutagenesis of the TATA box and upstream activator sequence in the haloarchaeal bop gene promoter. *J Bacteriol* 181, 2513-8.
- (39) Gropp, R., Gropp, F., and Betlach, M. C. (1992) Association of the halobacterial 7S RNA to the polysome correlates with expression of the membrane protein bacterioopsin. *Proc Natl Acad Sci US A* 89, 1204-8.
- (40) Arent, M. (2006), Seton Hall University.
- (41) Shine, J., and Dalgarno, L. (1974) The 3'-terminal sequence of *Escherichia coli* 16S ribosomal RNA: complementarity to nonsense triplets and ribosome binding sites. *Proc Natl Acad Sci US A* 71, 1342-6.
- (42) Sartorius-Neef, S., and Pfeifer, F. (2004) In vivo studies on putative Shine-Dalgarno sequences of the halophilic archaeon *Halobacterium salinarum*. *Mol Microbiol* 51, 579-88.
- (43) Kozak, M. (1991) Structural features in eukaryotic mRNAs that modulate the initiation of translation. *J Biol Chem* 266, 19867-70.
- (44) Dassarma, S., Rajbhandary, U. L., and Khorana, H. G. (1984) Bacterio-opsin mRNA in wild-type and bacterio-opsin-deficient *Halobacterium halobium* strains. *Proc Natl Acad Sci US A* 81, 125-129.
- (45) Moll, I., Grill, S., Gualerzi, C. O., and Blasi, U. (2002) Leaderless mRNAs in bacteria: surprises in ribosomal recruitment and translational control. *Mol Microbiol* 43, 239-46.
- (46) Ford, C. F., Suominen, I., and Glatz, C. E. (1991) Fusion tails for the recovery and purification of recombinant proteins. *Protein Expr Purif* 2, 95-107.
- (47) Turner, G. J., Reusch, R., Winter-Vann, A. M., Martinez, L., and Betlach, M. C. (1999) Heterologous gene expression in a membrane-protein-specific system. *Protein Expr Purif* 17, 312-23.
- (48) Bartus, C. L., Jaakola, V. P., Reusch, R., Valentine, H. H., Heikinheimo, P., Levay, A., Potter, L. T., Heimo, H., Goldman, A., and Turner, G. J. (2003) Downstream coding region determinants of bacterio-opsin, muscarinic acetylcholine receptor and adrenergic receptor expression in *Halobacterium salinarum*. *Biochim Biophys Acta* 1610, 109-23
- (49) Martinez, L. C., Thurmond, R. L., Jones, P. G., and Turner, G. J. (2002) Subdomains in the F and G helices of bacteriorhodopsin regulate the conformational transitions of the reprotonation mechanism. *Proteins* 48, 269-82.
- (50) Pfeifer, F., and Blaseio, U. (1990) Transposition burst of the ISH27 insertion element family in *Halobacterium halobium*. *Nucleic Acids Res* 18, 6921-5.
- (51) Lam, W. L., and Doolittle, W. F. (1992) Mevinolin-resistant mutations identify a promoter and the gene for a eukaryote-like 3-hydroxy-3-methylglutaryl-coenzyme

- A reductase in the archaeobacterium *Haloferax volcanii*. *J Biol Chem* 267, 5829-34.
- (52) Cline, S. W., Schalkwyk, L. C., and Doolittle, W. F. (1989) Transformation of the archaeobacterium *Halobacterium volcanii* with genomic DNA. *J Bacteriol* 171, 4987-91.
- (53) Martinez, L. C., and Turner, G. J. (2002) High-throughput screening of bacteriorhodopsin mutants in whole cell pastes. *Biochim Biophys Acta* 1564, 91-8.
- (54) Zuker, M. (2003) Mfold web server for nucleic acid folding and hybridization prediction. *Nucl. Acids Res.* 31, 3406-3415.
- (55) Srinivasan, G., Krebs, M. P., and RajBhandary, U. L. (2006) Translation initiation with GUC codon in the archaeon *Halobacterium salinarum*: implications for translation of leaderless mRNA and strict correlation between translation initiation and presence of mRNA. *Mol Microbiol* 59, 1013-24.
- (56) Xu, Z.-j., Moffett, D. B., Peters, T. R., Smith, L. D., Perry, B. P., Whitmer, J., Stokke, S. A., and Teintze, M. (1995) The Role of the Leader Sequence Coding Region in Expression and Assembly of Bacteriorhodopsin. *J. Biol. Chem.* 270, 24858-24863.
- (57) Simone, S.-N., and Felicitas, P. (2004) *In vivo* studies on putative Shine–Dalgarno sequences of the halophilic archaeon *Halobacterium salinarum*. *Molecular Microbiology* 51, 579-588.
- (58) Ivano, C., Andrea, C., Dario, B., Davide, R., and Paola, L. (1999) *Cis*-acting signals controlling translational initiation in the thermophilic archaeon *Sulfolobus solfataricus*. *Molecular Microbiology* 34, 377-384.
- (59) Brenneis, M., Hering, O., Lange, C., and Soppa, J. (2007) Experimental characterization of *Cis*-acting elements important for translation and transcription in halophilic archaea. *PLoS Genet* 3, e229.
- (60) Gayathri, S., Mark, P. K., and Uttam, L. R. (2006) Translation initiation with GUC codon in the archaeon *Halobacterium salinarum*: implications for translation of leaderless mRNA and strict correlation between translation initiation and presence of mRNA. *Molecular Microbiology* 59, 1013-1024.
- (61) Ni, B. F., Chang, M., Duschl, A., Lanyi, J., and Needleman, R. (1990) An efficient system for the synthesis of bacteriorhodopsin in *Halobacterium halobium*. *Gene* 90, 169-72.
- (62) Heymann, J. A., Havelka, W. A., and Oesterhelt, D. (1993) Homologous overexpression of a light-driven anion pump in an archaeobacterium. *Mol Microbiol* 7, 623-30.
- (63) Ferrando-May, E., Brustmann, B., and Oesterhelt, D. (1993) A C-terminal truncation results in high-level expression of the functional photoreceptor sensory rhodopsin I in the archaeon *Halobacterium salinarum*. *Mol Microbiol* 9, 943-53.
- (64) Krebs, M. P., Spudich, E. N., Khorana, H. G., and Spudich, J. L. (1993) Synthesis of a gene for sensory rhodopsin I and its functional expression in *Halobacterium halobium*. *Proc Natl Acad Sci US A* 90, 3486-90.
- (65) Grisshammer, R., and Tate, C. G. (1995) Overexpression of integral membrane proteins for structural studies. *Q Rev Biophys* 28, 315-422.
- (66) Tate, C. G., and Grisshammer, R. (1996) Heterologous expression of G-protein-coupled receptors. *Trends Biotechnol* 14, 426-30.

Annexure I

I. Concentrated Basal Salts (1 liter) – CBS

NaCl,	280 g
MgSO ₄ -7 H ₂ O,	23 g
Sodium Citrate-2 H ₂ O,	3.5 g
KCl,	2.3 g
1M Tris pH 7.4,	50mL

The 1M Tris buffer is titrated to pH 7.4 with concentrated HCL. Salts will dissolve faster if you add 140 g of NaCl + other ingredients and adjust the pH to 7.2 then add the remaining 140 g NaCl and adjust the pH again to 7.2. The solution is made in regular tap water and autoclaved for 20 minutes. The final pH of CBS should be 7.2.

II. Rich Halo-peptone medium (1 Liter) – RHM

875 ml concentrated basal salts

15 g oxoid peptone (or 100 ml 15% peptone solution in regular tap H₂O)

Adjust to 1 liter with tap H₂O

Titrate to pH 7.2 using NaOH and HCl.

15% peptone (1 liter)

Oxoid peptone, 150 g dissolved in 1 liter of dd water.

The solutions are autoclaved separately. Oxoid brand peptone is used because it contains very low amounts of bile salts, an inhibitory agent known to cause lysis of halobacteria (7).

A 15% solution of unautoclaved Oxoid peptone is difficult to sterilize by filtration due to fouling of the membrane with undissolved particulates. Autoclaving drives these particulates into solution and the peptone can then be filtered easily.

For 1 liter of complex medium, mix 875 ml of concentrated basal salts, 25 ml tap H₂O (not dd H₂O) and 100 ml 15 % peptone.

III. Rich Halo-yeast extract tryptone medium (YET)

For preparation of 10X YET (1Liter)

Bacto Tryptone 50 g.

Bacto Yeast 30 g.

Regular tap H₂O to 1L.

Mix all the ingredients and autoclave for 20 minutes.

IV. Diluted basal salts (100 ml)

87.5 ml concentrated basal salts

12.5 ml regular tap H₂O

V. Halo Peptone Plates 1 Liter solution

Concentrated Basal Salts 875 ml

15% Oxoid Peptone 100 ml

Regular tap H₂O 25 ml

Oxoid Agar 15 g

The CBS and the 15% oxoid peptone are added and the solution is brought to 1 liter using regular tap water. The pH is adjusted to 7.2 (6.9 to 7.2). To this solution 15g of Oxoid agar is added and autoclaved for 10 minutes. The solution is allowed to cool in a 55 °C water bath and the plates are poured immediately.

For mevinolin plates add 750 ul of 10mM Mevinolin stock solution to the autoclaved solution after cooling.

Halobium Transformation Solutions

VII. Spheroplasting Solution: (pH 8.75)

<u>Reagent</u>	<u>Concentration</u>	<u>g/100ml</u>
Sucrose	15%	15
NaCl	2M	11.69
KCl	27mM	0.201
Tris-HCl	50mM	0.790

Titrate with NaOH

VIII. Spheroplasting Solution with EDTA: (pH 8.0)

<u>Reagent</u>	<u>Concentration</u>	<u>g/100ml</u>
(Na) ₄ EDTA	0.5M	19
Sucrose	15%	15
NaCl	2M	11.69
KCl	27mM	0.201
Tris-HCl	50mM	0.790

Titrate with HCl

IX. Spheroplast Diluting Solution: (pH 7.4)

<u>Reagent</u>	<u>Concentration</u>	<u>g/100ml</u>
Sucrose	15%	15
CBS	87.5ml	
Tris-HCl	50mM	0.790

X. PEG

PEG(600)	Spheroplasting Solution
3ml	2ml

PEG solution is made fresh each time. Equal volumes of spheroplast suspension and PEG are mixed to give a final concentration of 30%.

XI. DNA (for Halo transformations):

One microgram of DNA is suspended in 10uL spheroplasting solution.

Bacterial plates

All plates must be made with strict sterile technique. After pouring, leave plates to dry at RT for 1-2 days, then store upside-down in plastic bags in the cold room. Plates should be clearly marked on the outside with colors indicated. Close the bags with tape, mark and date each bag.

LB plates (To make 4 litres)

40 g Bacto Tryptone

20 g Bacto Yeast extract

40 g NaCl

Make up in 3200 ml dH₂O.

Adjust pH from ~6.9 to 7.5 with 12-14 ml of 1 M NaOH

Bring volume to 4 l.

Add 60 g Bacto-agar, mix, autoclave.

When agar has cooled to 55°C, pour plates (~25 ml per large plate). If you can keep your hand on the side of the flask then it is cool enough.

Mark LB sides with **GREEN** stripe.

LB Amp plates (75 mg/ml Ampicillin)

Follow protocol for LB plates until after autoclaving. When agar has cooled to 55°C, add 4 ml (2 vials) of 75 mg/ml Ampicillin stock (1000X stock, kept at -20°C). Pour plates as above. Amp plates marked with **RED** stripe.

Ampicillin is unstable. Plates older than four months cannot be used—so don't make up too much at any one time.

Annexre II.

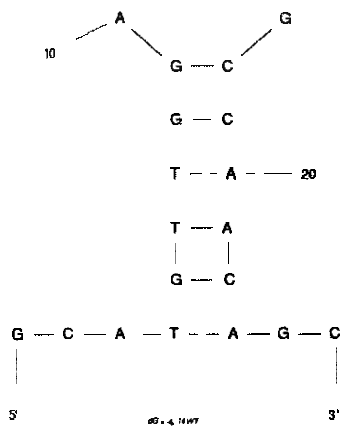
I. WT - GCATGTTGGAGTTATTGCCAACAGC - Structure 1

$\Delta G^0 = -4.14$ kcal/mol at 37 °C

$\Delta H^0 = -49.50$ kcal/mol

$\Delta S^0 = -146.2$ cal/ (K·mol)

$T_m = 65.3$ °C assuming a 2 state model.



Structural element	δG	Information
	-0.46	5 ss bases & 1 closing helices.
	-1.45	External closing pair is T ⁴ -A ²³
	-1.44	External closing pair is G ⁵ -C ²²
	-1.00	External closing pair is T ⁶ -A ²¹
Stack	-1.45	External closing pair is T'-A ²⁰
Stack	-1.84	External closing pair is G ⁸ -C ¹⁹
Helix	-7.18	6 base pairs.
Hairpin loop	3.50	Closing pair is G ⁹ -C ¹⁸

Table 3 a (i): The Mfold thermodynamics predictions for WT

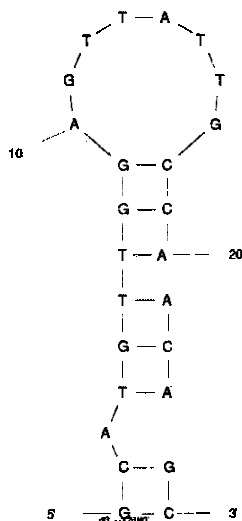
WT - Structure 2 :

$\Delta G^0 = -3.20$ kcal/mol at 37 °C

$\Delta H^0 = -62.30$ kcal/mol

$\Delta S^0 = -190.5$ cal/ (K·mol)

$T_m = 53.7$ °C assuming a 2 state model



Structural element	δG	Information
External loop	0.00	0 ss bases & 1 closing helices.
Stack	-2.24	External closing pair is G ¹ -C ²⁵
Helix	-2.24	2 base pairs.
Bulge loop	2.72	External closing pair is C ² -G ²⁴
Stack	-1.45	External closing pair is T ⁴ -A ²³
Stack	-1.44	External closing pair is G ⁵ -C ²²
Stack		External closing pair is T ⁶ -A ²¹
Stack	-1.45	External closing pair is T ⁷ -A ²⁰
Stack	-1.84	External closing pair is G ⁸ -C ¹⁹
Helix	-7.18	6 base pairs.
Hairpin loop		Closing pair is G ⁹ -C ¹⁸

Table 3 a (ii): The Mfold thermodynamics predictions for WT

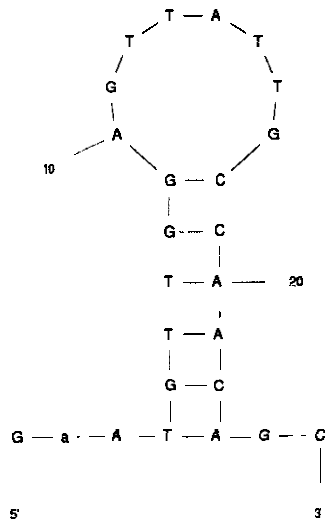
II C2A–Structure 1 - GaATGTTGGAGTTATTGCCAACAGC

$\Delta G^0 = -4.14$ kcal/mol at 37 °C

$\Delta H^0 = -49.50$ kcal/mol

$\Delta S^0 = -146.2$ cal/ (K·mol)

$T_m = 65.3$ °C assuming a 2 state model



Structural element	δG	Information
External loop	-0.46	5 ss bases & 1 closing helices.
Stack	-1.45	External closing pair is T ⁴ -A ²³
Stack	-1.44	External closing pair is G ⁵ -C ²²
Stack	-1.00	External closing pair is T ⁶ -A ²¹
Stack	-1.45	External closing pair is T ⁷ -A ²⁰
Stack	-1.84	External closing pair is G ⁸ -C ¹⁹
Helix	-7.18	6 base pairs.
Hairpin loop	3.50	Closing pair is G ⁹ -C ¹⁸

Table 3 b: The Mfold thermodynamics predictions for C2A

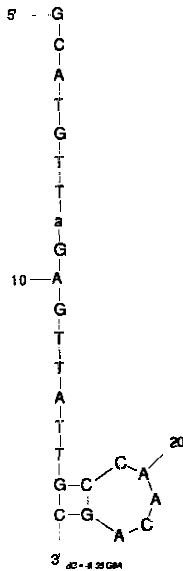
III. G8A= Structure 1 – GCATGTTaGAGTTATTGCCAACAGC

$\Delta G^0 = -0.35$ kcal/mol at 37 °C

$\Delta H^0 = -17.10$ kcal/mol

$\Delta S^0 = -54$ cal/ (K·mol)

$T_m = 43.4$ °C assuming a 2 state model



Information

External loop	-0.61	16 ss bases & 1 closing helices.
Stack	-2.24	External closing pair is G ¹⁷ -C ²⁵
Helix	-2.24	2 base pairs.
Hairpin loop	2.50	Closing pair is C ¹⁸ -G ²⁴

Table 3 c (i): The Mfold thermodynamics predictions for G8A

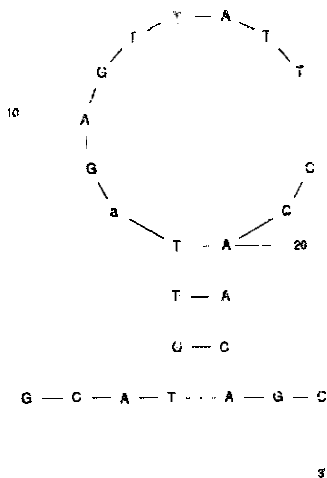
G8A – Structure 2

$\Delta G^0 = -0.25$ kcal/mol at 37 °C

$\Delta H^0 = -32.20$ kcal/mol

$\Delta S^0 = -103$ cal/ (K·mol)

$T_m = 39.4$ °C assuming a 2 state model



Structural element	δG	Information
External loop	-0.46	5 ss bases & 1 closing helices.
Stack	-1.45	External closing pair is T ⁴ -A ²³
Stack	-1.44	External closing pair is G ⁵ -C ²²
Stack	-1.00	External closing pair is T ⁶ -A ²¹
Helix	-3.89	4 base pairs.
Hairpin loop	4.10	Closing pair is T ⁷ -A ²⁰

Table 3 c (ii): The Mfold thermodynamics predictions for G8A

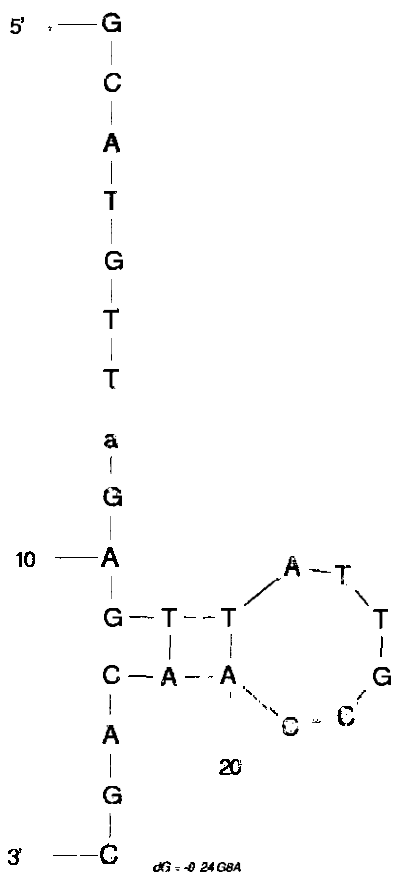
G8A -- Structure 3

$$\Delta G^0 = -0.24 \text{ kcal/mol at } 37 \text{ }^\circ\text{C}$$

$$\Delta H^0 = -28.50 \text{ kcal/mol}$$

$$\Delta S^0 = -91.1 \text{ cal/ (K}\cdot\text{mol)}$$

$$T_m = 39.6 \text{ }^\circ\text{C assuming a 2 state model}$$



Structural element	δG	Information
External loop	-1.40	13 ss bases & 1 closing helices.
Stack	-1.44	External closing pair is G ¹¹ -C ²²
	-1.00	External closing pair is T ¹² -A ²¹
Helix	-2.44	3 base pairs.
Hairpin loop	3.60	Closing pair is T ¹³ -A ²⁰

Table 3 c (iii): The Mfold thermodynamics predictions for G8A

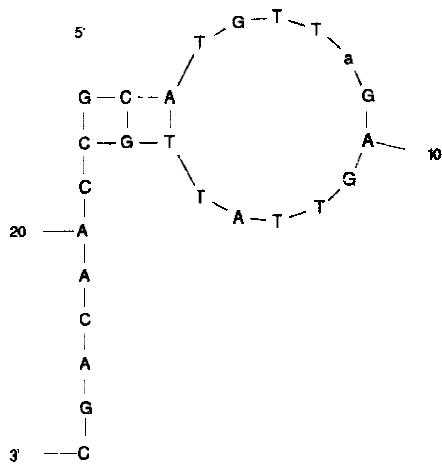
G8A – Structure 4

$$\Delta G^0 = 0.10 \text{ kcal/mol at } 37 \text{ }^\circ\text{C}$$

$$\Delta H^0 = -23.30 \text{ kcal/mol}$$

$$\Delta S^0 = -75.4 \text{ cal/ (K}\cdot\text{mol)}$$

$$T_m = 35.6 \text{ }^\circ\text{C assuming a 2 state model}$$



Structural element	δG	Information
External loop	-0.31	7 ss bases & 1 closing helices.
Stack	-2.24	External closing pair is G ¹ -C ¹⁸
Stack	-1.45	External closing pair is C ² -G ¹⁷
Helix	-3.69	3 base pairs.
Hairpin loop	4.10	Closing pair is A ³ -T ¹⁶

Table 3 c (iv): The Mfold thermodynamics predictions for G8A

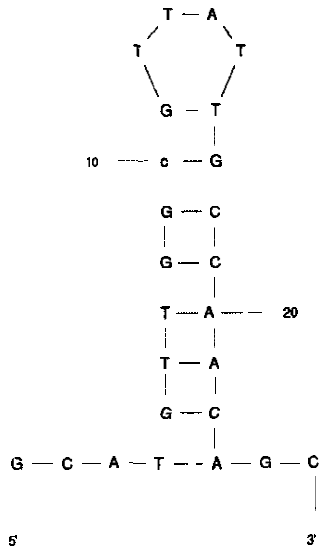
A10C -- Structure 1- GCATGTTGGcGTTATTGCCAACAGC

$\Delta G^0 = -7.05$ kcal/mol at 37 °C

$\Delta H^0 = -60.00$ kcal/mol

$\Delta S^0 = -170.7$ cal/ (K.mol)

$T_m = 78.2$ °C assuming a 2 state model



Structure

External

Stack	.45	External closing pair is T ⁴ -A ²³
Stack	-1.44	External closing pair is G ⁵ -C ²²
Stack	-1.00	External closing pair is T ⁶ -A ²¹
Stack	-1.45	External closing pair is T ⁷ -A ²⁰
Stack		ernal closing pair is G ⁸ -C ¹⁹
Stack		External closing pair is G ⁹ -C ¹⁸
Stack	-0.47	External closing pair is c ¹⁰ -G ¹⁷
Helix	-9.89	8 base pairs.
Hairpin loop	3.30	Closing pair is G ¹¹ -T ¹⁶

Table 3 d (i): The Mfold thermodynamics predictions for A10C

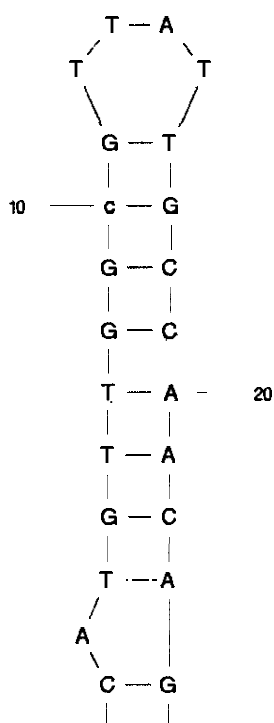
A10C – Structure 2

$\Delta G^0 = -6.11$ kcal/mol at 37 °C

$\Delta H^0 = -72.80$ kcal/mol

$\Delta S^0 = -215$ cal/ (K·mol)

$T_m = 65.4$ °C assuming a 2 state model



Structural element	δG	Information
External loop		ss bases & 1 closing helices.
Stack	-2.24	External closing pair is G ¹ -C ²⁵
Helix	-2.24	2 base pairs.
Bulge loop	2.72	External closing pair is C ² -G ²⁴
Stack	-1.45	External closing pair is T ⁴ -A ²³
Stack	-1.44	External closing pair is G ⁵ -C ²²
Stack	-1.00	External closing pair is T ⁶ -A ²¹
Stack	-1.45	External closing pair is T ⁷ -A ²⁰
Stack	-1.84	External closing pair is G ⁸ -C ¹⁹
Stack	-2.24	External closing pair is G ⁹ -C ¹⁸
Stack	-0.47	External closing pair is c ¹⁰ -G ¹⁷
Helix	-9.89	8 base pairs.
Hairpin loop	3.30	Closing pair is G ¹¹ -T ¹⁶

Table 3 d (ii): The Mfold thermodynamics predictions for A10C

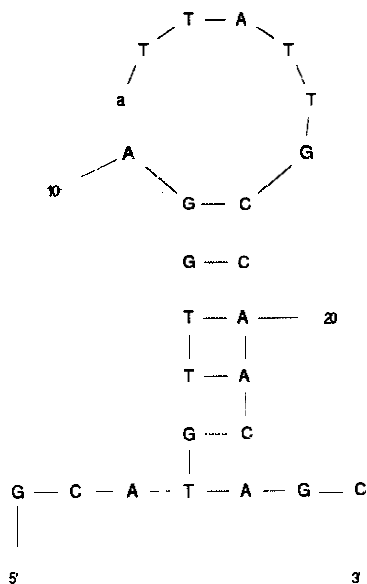
G11A – Structure 1 – GCATGTTGGAaTTATTGCCAACAGC

$\Delta G^0 = -4.14$ kcal/mol at 37 °C

$\Delta H^0 = -49.50$ kcal/mol

$\Delta S^0 = -146.2$ cal/ (K·mol)

$T_m = 65.3$ °C assuming a 2 state model



Structural element	δG	Information
External loop	-0.46	5 ss bases & 1 closing helices.
Stack	-1.45	External closing pair is T ⁴ -A ²³
Stack	-1.44	External closing pair is G ⁵ -C ²²
Stack	-1.00	External closing pair is T ⁶ -A ²¹
Stack	-1.45	External closing pair is T ⁷ -A ²⁰
Stack	-1.84	External closing pair is G ⁸ -C ¹⁹
Helix	8	6 base pairs.
Hairpin loop	3.50	Closing pair is G ⁹ -C ¹⁸

Table 3 e (i): The Mfold thermodynamics predictions for G11A

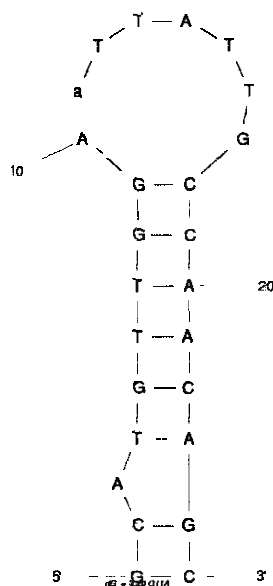
G11A-Structure 2

$\Delta G^0 = -3.20$ kcal/mol at 37 °C

$\Delta H^0 = -62.30$ kcal/mol

$\Delta S^0 = -190.5$ cal/ (K·mol)

$T_m = 53.7$ °C assuming a 2 state model



Structural element	δG	Information
External loop	0.00	0 ss bases & 1 closing helices.
Stack	-2.24	External closing pair is G ¹ -C ²⁵
Helix	-2.24	2 base pairs.
Bulge loop	2.72	External closing pair is C ² -G ²⁴
Stack	-1.45	External closing pair is T ⁴ -A ²³
Stack	-1.44	External closing pair is G ⁵ -C ²²
Stack	-1.00	External closing pair is T ⁶ -A ²¹
Stack	-1.45	External closing pair is T ⁷ -A ²⁰
Stack	-1.84	External closing pair is G ⁸ -C ¹⁹
Helix	-7.18	6 base pairs.
Hairpin loop	3.50	Closing pair is G ⁹ -C ¹⁸

Table 3 e (ii): The Mfold thermodynamics predictions for G11A

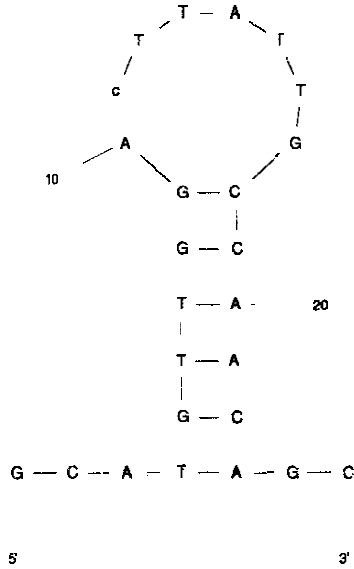
G11C – Structure 1 - GCATGTTGGAcTTATTGCCAACAGC

$\Delta G^0 = -4.14$ kcal/mol at 37 °C

$\Delta H^0 = -49.50$ kcal/mol

$\Delta S^0 = -146.2$ cal/ (K·mol)

$T_m = 65.3$ °C assuming a 2 state model



Structural element	δG	Information
External loop		5 ss bases & 1 closing helices.
Stack	-1.45	External closing pair is T ⁴ -A ²³
Stack	-1.44	External closing pair is G ⁵ -C ²²
Stack	-1.00	External closing pair is T ⁶ -A ²¹
Stack		External closing pair is T ⁷ -A ²⁰
Stack	-1.84	External closing pair is G ⁸ -C ¹⁹
Helix	-7.18	6 base pairs.
Hairpin loop	3.50	Closing pair is G ⁹ -C ¹⁸

Table 3 f (i): The Mfold thermodynamics predictions for G11 C

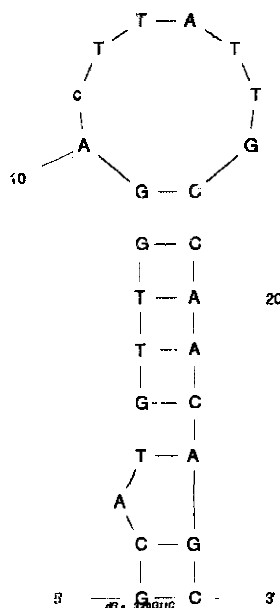
G11C - Structure 2

$\Delta G^0 = -3.20$ kcal/mol at 37 °C

$\Delta H^0 = -62.30$ kcal/mol

$\Delta S^0 = -190.5$ cal/ (K·mol)

$T_m = 53.7$ °C assuming a 2 state model



Structural element	δG	Information
External loop	0.00	0 ss bases & 1 closing helices.
Stack	-2.24	External closing pair is G ¹ -C ²⁵
Helix	-2.24	2 base pairs.
Bulge loop	2.72	External closing pair is C ² -G ²⁴
Stack	-1.45	External closing pair is T ⁴ -A ²³
Stack	-1.44	External closing pair is G ⁵ -C ²²
Stack	-1.00	External closing pair is T ⁶ -A ²¹
Stack	-1.45	External closing pair is T ⁷ -A ²⁰
Stack	-1.84	External closing pair is G ⁸ -C ¹⁹
Helix		
Hairpin loop	3.50	Closing pair is G ⁹ -C ¹⁸

Table 3 f (ii): The Mfold thermodynamics predictions for G11C

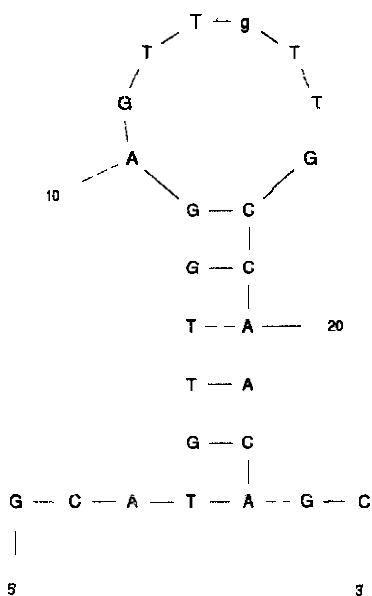
A14G– GCATGTTGGAGTTgTTGCCAACAGC - Structure 1

$\Delta G^0 = -4.14$ kcal/mol at 37 °C

$\Delta H^0 = -49.50$ kcal/mol

$\Delta S^0 = -146.2$ cal/ (K mol)

$T_m = 65.3$ °C assuming a 2 state model



Structural element	δG	Information
External loop	-0.46	5 ss bases & 1 closing helices.
Stack	-1.45	External closing pair is T ⁴ -A ²³
Stack	-1.44	External closing pair is G ⁵ -C ²²
Stack	-1.00	External closing pair is T ⁶ -A ²¹
Stack	-1.45	External closing pair is T ⁷ -A ²⁰
Stack	-1.84	External closing pair is G ⁸ -C ¹⁹
Helix	-7.18	6 base pairs.
Hairpin loop	3.50	Closing pair is G ⁹ -C ¹⁸

Table 3 g (i): The Mfold thermodynamics predictions for A14G

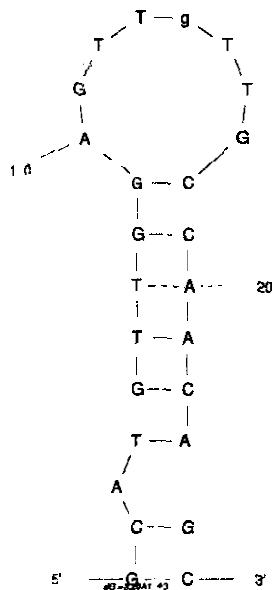
A14G – Structure 2

$$\Delta G^0 = -3.20 \text{ kcal/mol at } 37 \text{ }^\circ\text{C}$$

$$\Delta H^0 = -62.30 \text{ kcal/mol}$$

$$\Delta S^0 = -190.5 \text{ cal/ (K}\cdot\text{mol)}$$

$$T_m = 53.7 \text{ }^\circ\text{C assuming a 2 state model}$$



Information		
	0.00	0 ss bases & 1 closing helices.
Stack	-2.24	External closing pair is G ¹ -C ²⁵
Helix	-2.24	2 base pairs.
Bulge loop	2.72	External closing pair is C ² -G ²⁴
Stack	-1.45	External closing pair is T ⁴ -A ²³
Stack	-1.44	External closing pair is G ⁵ -C ²²
Stack	-1.00	External closing pair is T ⁶ -A ²¹
Stack	-1.45	External closing pair is T ⁷ -A ²⁰
Stack	-1.84	External closing pair is G ⁸ -C ¹⁹
Helix	-7.18	6 base pairs.
Hairpin loop	3.50	Closing pair is G ⁹ -C ¹⁸

Table 3 g (ii): The Mfold thermodynamics predictions for A14G

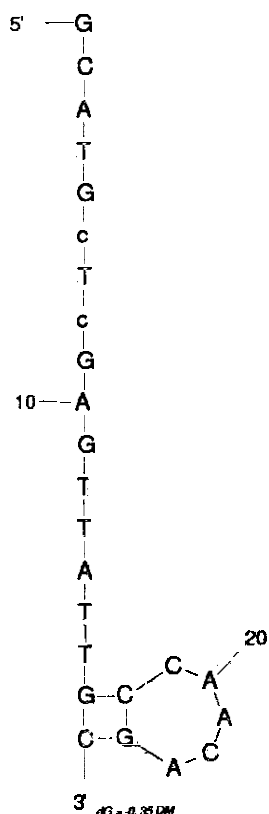
DM- GCATGcTcGAGTTATTGCCAACAGC–Structure 1

$\Delta G^0 = -0.35$ kcal/mol at 37 °C

$\Delta H^0 = -17.10$ kcal/mol

$\Delta S^0 = -54$ cal/ (K·mol)

$T_m = 43.4$ °C assuming a 2 state model



Structural element	δG	Information
External loop	-0.61	16 ss bases & 1 closing helices.
Stack	-2.24	External closing pair is G ¹⁷ -C ²⁵
Helix		2 base pairs.
Hairpin loop	2.50	Closing pair is C ¹⁸ -G ²⁴

Table 3 h (i): The Mfold thermodynamics predictions for DM

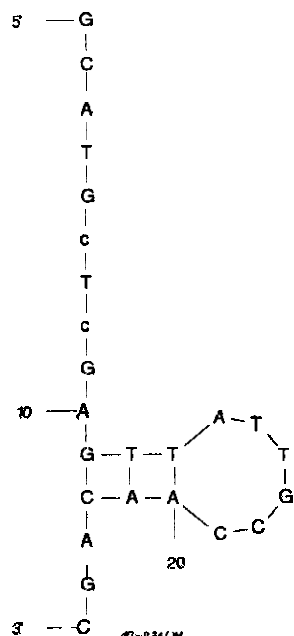
DM – Structure 2

$\Delta G^0 = -0.24$ kcal/mol at 37 °C

$\Delta H^0 = -28.50$ kcal/mol

$\Delta S^0 = -91.1$ cal/ (K·mol)

$T_m = 39.6$ °C assuming a 2 state model



Structural element	δG	Information
External loop	-1.40	13 ss bases & 1 closing helices.
Stack	-1.44	External closing pair is G ¹¹ -C ²²
Stack	-1.00	External closing pair is T ¹² -A ²¹
Helix	-2.44	3 base pairs.
Hairpin loop	3.60	Closing pair is T ¹³ -A ²⁰

Table 3 h (ii): The Mfold thermodynamics predictions for DM

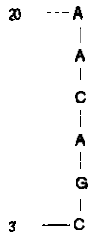
DM – Structure 3

$\Delta G^0 = 0.10$ kcal/mol at 37 °C

$\Delta H^0 = -23.30$ kcal/mol

$\Delta S^0 = -75.4$ cal/ (K·mol)

$T_m = 35.6$ °C assuming a 2 state model



Structural element	δG	Information
External loop	-0.31	7 ss bases & 1 closing helices.
Stack	-2.24	External closing pair is G ¹ -C ¹⁸
Stack	-1.45	External closing pair is C ² -G ¹⁷
Helix	-3.69	3 base pairs.
Hairpin loop	4.10	Closing pair is A ³ -T ¹⁶

Table 3 h (iii): The Mfold thermodynamics predictions for DM

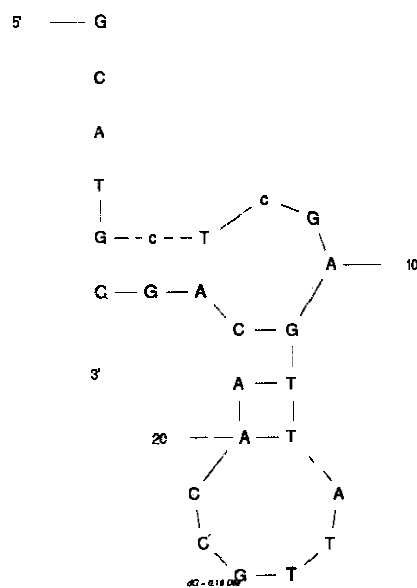
DM – Structure 4

$\Delta G^0 = 0.18$ kcal/mol at 37 °C

$\Delta H^0 = -39.20$ kcal/mol

$\Delta S^0 = -126.9$ cal/ (K·mol)

$T_m = 35.5$ °C assuming a 2 state model



Structural element	δG	Information
External loop	-0.61	4 ss bases & 1 closing helices.
Stack	-2.24	External closing pair is G ⁵ -C ²⁵
Stack	-1.28	External closing pair is C ⁶ -G ²⁴
Helix	-3.52	3 base pairs.
Bulge loop	3.15	External closing pair is T ⁷ -A ²³
Stack		External closing pair is G ¹¹ -C ²²
Stack	-1.00	External closing pair is T ¹² -A ²¹
Helix	-2.44	3 base pairs.
Hairpin loop	3.60	Closing pair is T ¹³ -A ²⁰

Table 3 h (iv): The Mfold thermodynamics predictions for DM

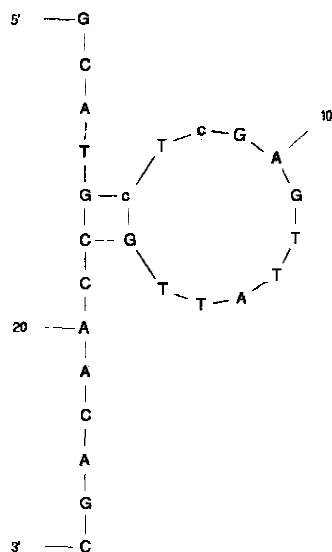
DM – Structure 5

$\Delta G^0 = 0.24$ kcal/mol at 37 °C

$\Delta H^0 = -22.60$ kcal/mol

$\Delta S^0 = -73.6$ cal/ (K·mol)

$T_m = 33.7$ °C assuming a 2 state model



Structural element	δG	Information
External loop		11 ss bases & 1 closing helices.
Stack	-2.24	External closing pair is G ⁵ -C ¹⁸
Helix	-2.24	2 base pairs.
Hairpin loop	3.40	Closing pair is c ⁶ -G ¹⁷

Table 3 h (v): The Mfold thermodynamics predictions for DM

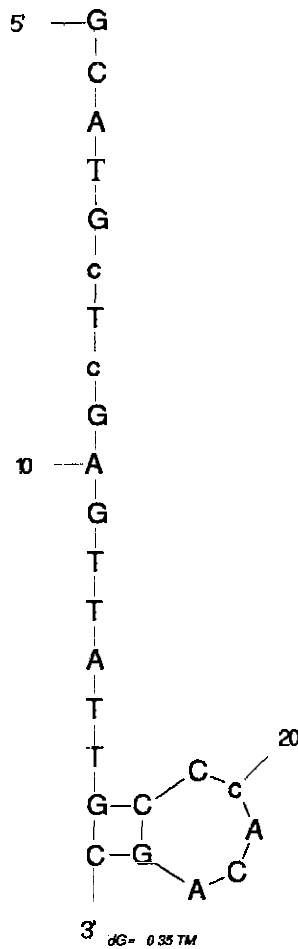
TM - GCATGcTcGAGTTATTGCCcACAGC—Structure 1

$\Delta G^0 = -0.35$ kcal/mol at 37 °C

$\Delta H^0 = -17.10$ kcal/mol

$\Delta S^0 = -54$ cal/ (K·mol)

$T_m = 43.4$ °C assuming a 2 state model



Structural element	δG	Information
External loop	-0.61	16 ss bases & 1 closing helices.
Stack	-2.24	External closing pair is G ¹⁷ -C ²⁵
Helix	-2.24	2 base pairs.
Hairpin loop	2.50	Closing pair is C ¹⁸ -G ²⁴

Table 3 i (i): The Mfold thermodynamics predictions for TM

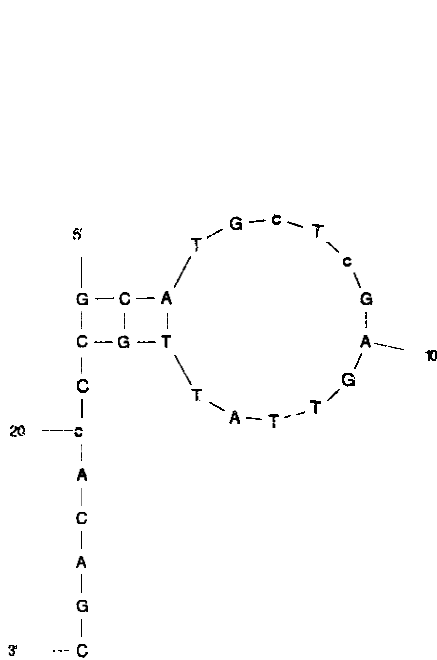
TM – Structure 2

$\Delta G^0 = 0.10$ kcal/mol at 37 °C

$\Delta H^0 = -23.30$ kcal/mol

$\Delta S^0 = -75.4$ cal/ (K·mol)

$T_m = 35.6$ °C assuming a 2 state model



Structural element	δG	Information
External loop	-0.31	7 ss bases & 1 closing helix
Stack	-2.24	External closing pair is G ¹ -C ¹⁸
Stack	-1.45	External closing pair is C ² -G ¹⁷
Helix	-3.69	3 base pairs.
Hairpin loop	4.10	Closing pair is A ³ -T ¹⁶

Table 3 i (ii): The Mfold thermodynamics predictions for TM

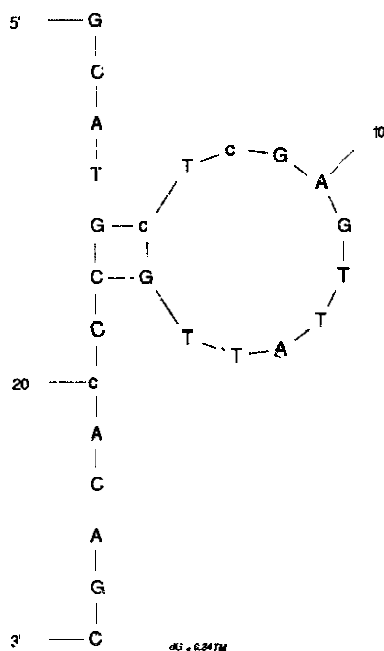
TM – Structure 3

$$\Delta G^0 = 0.24 \text{ kcal/mol at } 37 \text{ }^\circ\text{C}$$

$$\Delta H^0 = -22.60 \text{ kcal/mol}$$

$$\Delta S^0 = -73.6 \text{ cal/ (K mol)}$$

$$T_m = 33.7 \text{ }^\circ\text{C assuming a 2 state model}$$



Structural element	δG	Information
External loop	-0.92	11 ss bases & 1 closing helices.
Stack	-2.24	External closing pair is G ⁵ -C ¹⁸
Helix	-2.24	2 base pairs.
Hairpin loop	3.40	Closing pair is c ⁶ -G ¹⁷

Table 3 i (iii): The Mfold thermodynamics predictions for TM

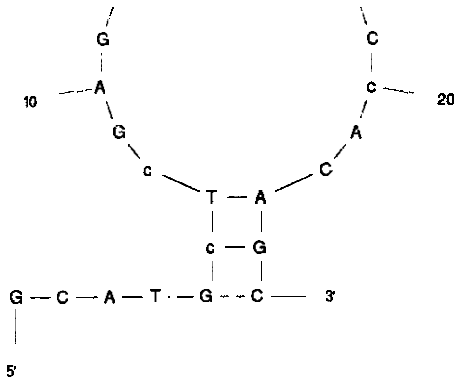
TM – Structure 4

$\Delta G^0 = 0.37$ kcal/mol at 37 °C

$\Delta H^0 = -23.00$ kcal/mol

$\Delta S^0 = -75.3$ cal/ (K·mol)

$T_m = 32$ °C assuming a 2 state model



Structural element	δG	Information
External loop	-0.61	4 ss bases & 1 closing helices.
Stack	-2.24	External closing pair is C ⁵ -C ²⁵
Stack	-1.28	External closing pair is C ⁶ -G ²⁴
Helix	-3.52	3 base pairs.
Hairpin loop	4.50	Closing pair is T ⁷ -A ²³

Table 3 i (iv): The Mfold thermodynamics predictions for TM